Planetary and Space Science 152 (2018) 116–135

Contents lists available at ScienceDirect

Planetary and Space Science

journal homepage: www.elsevier.com/locate/pss

Photometric survey and taxonomic identifications of 92 near-Earth asteroids

Chien-Hsien Lin [a,c], Wing-Huen Ip [a,b,*], Zhong-Yi Lin [b], Yu-Chi Cheng [b], Hsing-Wen Lin [b], Chan-Kao Chang [b]

[a] Space Science Institute, Macau University of Science and Technology, Macau S.A.R., China
[b] Institute of Astronomy, National Central University, Taoyuan, Taiwan
[c] Key Laboratory for the Structure and Evolution of Celestial Objects, Chinese Academy of Science, Kumming, Yunnan, China

ARTICLE INFO

Keywords:
Near-Earth asteroids
Photometry
Taxonomy

ABSTRACT

A photometric survey of near-Earth asteroids (NEAs) was conducted from 2012 through 2014 at Lulin Observatory, Taiwan. The measurements of the color indices, B-V, V-R, and V-I allow the classification of 92 NEAs into seven taxonomic types. Of these samples, 39 of them are new classifications. The fractional abundances of these taxonomic complexes are: A ~3%, C~6.5%, D~8%, Q~26%, S~37%, V~6.5%, and X~13%. This result is similar to that of Thomas et al. (2011) even though the populations of the D- and X-complex with low albedos are underrepresented. The ratio of the C-cluster to the total population of S + C clusters are 0.22 ± 0.06 for H ≤ 17.0 and 0.31 ± 0.06 for H > 17.0, indicating a slightly higher fraction of dark-object population with sizes smaller than 1 km.

1. Introduction

The asteroidal population is characterized by different chemical compositions and taxonomic types at different heliocentric distances. The S-type asteroids can be found most often in the inner asteroid belt while the C-type asteroids dominate the outer belt population (Tholen, 1984; Bus and Binzel, 2002; DeMeo et al., 2009; DeMeo and Carry, 2013). The Near-Earth Asteroids (NEAs) with orbits near or crossing the Earth's orbit are products of collisional fragmentation of main belt parent bodies. How these small pieces of km to sub-km size range can be transported from the main belt to the Mars and Earth crossing orbits via the 3:1 mean motion resonance, ν6 secular resonance, or the Yarkovsky effect has been investigated in detail by a number of authors (Bottke et al., 2002; Morbidelli and Vokrouhlicky', 2003; Greenstreet et al., 2012; Granvik et al., 2016). The taxonomic mapping of NEAs can therefore provide important information on their source regions and evolutionary histories (DeMeo and Carry, 2014; Carry et al., 2016).

On the basis of the Bus-system (Bus, 1999), several observational studies have shown that the S, Q, X and C-complexes in total account for about 90% of the NEA population while the rest is comprised of the A, D and V types (Dandy et al., 2003; Binzel et al., 2004; de Leo'n et al., 2010; Ye, 2011; Thomas et al., 2011).

The C-type and D-type NEAs are of special interest because of their volatile contents (Nichols, 1993; Reddy et al., 2012a). The C-type NEAs are likely originated from the outer main belt which is known to be the reservoir of asteroids of carbonaceous composition (Bus and Binzel, 2002; DeMeo and Carry, 2014) and the so-called main belt comets with active outgassing phenomenon (Hsieh and Jewitt, 2006; Bertini, 2011). At the same time, the D-type and P-type NEAs could be of cometary origin (Jones et al., 1990; Rivkin, 2006; Volquardsen, 2007). The D-type objects are rather rare in the NEA population (Perna et al., 2016). Search for these volatile-rich NEAs as potential targets for future space missions is one of the scientific goals of the Lulin photometric survey.

Some S-type and Q-type are likely the same as ordinary chondritic composition (Tholen, 1984; Vernazza et al., 2008). That the S-type asteroids are redder and darker than the Q-type asteroids implies with the higher level of space weathering effect (Brunetto et al., 2006, 2015; Clark et al., 2002; Ishiguro et al., 2007). This also means that the Q-type asteroids should have younger (fresher) surfaces. The direct evidence of space weathering on surface particles has been derived from asteroid Itokawa from Hayabusa mission (Nakamura et al., 2011; Brunetto et al., 2015) Comparisons of the Q/S ratios in the main belt and the NEA population (Bus and Binzel, 2002; Lazzaro et al., 2004; Binzel et al., 2004; Dandy et al., 2003; Lin et al., 2015) have led to the interpretation that some physical mechanism must be at work to rejuvenate the surfaces of the Q-type objects once being injected into the orbital region of the terrestrial planets. Seismic shaking or removal of the surface materials by tidal effect during close encounters with the Earth and Venus has been

* Corresponding author. Space Science Institute, Macau University of Science and Technology, Macau S.A.R., China.
E-mail address: wingip@astro.ncu.edu.tw (W.-H. Ip).

https://doi.org/10.1016/j.pss.2017.12.019
Received 17 May 2017; Received in revised form 18 December 2017; Accepted 31 December 2017
Available online 4 January 2018
0032-0633/© 2018 Elsevier Ltd. All rights reserved.

proposed and apparently supported by numerical studies showing that the Q-type NEAs tended to have more close encounters with the Earth and Venus than the S-type NEAs (Binzel et al., 2010; Nesvorny et al., 2010; Carry et al., 2016). DeMeo et al. (2014) even added that Mars could also be important for such surface rejuvenation process, yet Carry et al. (2016) did not found the significant difference in orbital properties of Q- and S-types in their encounters with Mars.

Another mechanism of potential importance has to do with the YORP effect of asteroidal rotation (Rubincam, 2000). The increase of the rotational rate because of the YORP effect to a certain critical value upon which the surface materials would be either spun off (Jacobson and Scheeres, 2011; Polishook et al., 2014) or turned over (Walsh et al., 2012; Scheeres, 2015) could play a role in keeping a higher Q/S ratio (Graves et al., 2016).

Of the 14,000 NEAs discovered up to now, only 800 have been classified by spectroscopic observations (Binzel et al., 2002: Data Base of Physical and Dynamical Properties of NEAs on E.A.R.N.) and 300 by photometric measurements in terms of color indices from SDSS (Carry et al., 2016) and the Bessel system photometry (Rabinowitz, 1998; Binzel et al., 2002 (NEA database); Dandy et al., 2003; Ye, 2011). Therefore there is a need to acquire more taxonomic data so that a number of major issues in NEAs as discussed above can be addressed.

2. Previous studies on the boulder shape and destruction mechanisms

2.1. Procedure

The 2012–2014 observations were carried out monthly at the Lulin Observatory in the middle of Taiwan (latitude = 23° 28′ 07” N, longitude = 120° 52′ 25” E and altitude = 2862 m) using either the Lulin One-meter Telescope (LOT) or the Super Light Telescope (SLT) with a primary mirror of 41 cm. The CCD camera installed on LOT was PI-1300 which has a field of view (FOV) of 11'×11′ and an effective pixel scale of 0.516”/pxl; the one on SLT was U42 with FOV of 27'×27′ and a pixel scale of 0.78”/pxl. The filters for both telescopes were Bessel broad-band BVRI filters with central wavelengths at 442, 540, 647 and 786 nm, respectively. Our observational strategy was to select NEAs with visible magnitude brighter than 19.0 in each month irrespective of whether their taxonomical classifications were known or not. All data sets considered had been obtained with air mass below 2.0. About 30% of the observations – 21 out of 92 our NEAs - were conducted with the color sequence as RBRVRIR especially for those brighter targets whose exposure time was able to be acquired in shorter time duration, while others were obtained simply with the sequence as BVRI for most of long exposures. The observational log can be found in Appendix A.

2.2. Data reduction

The observations in each night had their own set of Landolt standard stars used for flux calibration (Landolt, 1992). The routine procedure of fitting for air mass extinction and imaging photometry was performed by using the IRAF package (Image Reduction and Analysis Facility supplied by National Optical Astronomy Observatories); the WCS information on the images was applied with the code from astrometry.net (Lang et al., 2010). Some observational data in specific dates were excluded from observation log (Appendix A) because of bad extinction value for color calibration, background star eclipse by the target NEAs, or photometric error with magnitude $\Delta m > 0.15$. Each target has at least once full BVRI exposures. There are some targets with multiple serial exposures as requested.

2.3. Color indices

The absolute magnitudes (H) of our NEA targets ranged from 9.45 to 21.8. This means that some of the observations were done during the close approaches of the NEAs to the Earth. The apparent brightness of each band was derived from aperture photometry. The color indices were then computed for B-V, V-R and V-I. For multiple sets of BVRI exposures, the average values are used. The results are summarized in Table 1. Note that five NEAs in the table have one missing color index because of stellar eclipse during individual observations. Overall, the Bessel color indices for 64 of the NEAs are derived for the first time from this work.

3. Taxonomic classifications

3.1. Integrated classes

The definition of asteroidal spectral types we used here is the Bus-DeMeo system (DeMeo et al., 2009). However, the broad-band photometry employed cannot give high resolution data as spectroscopic observations do, and our measurements were also limited in the optical wavelength range, without near-infrared coverage. We therefore made use of the classification scheme given by Binzel et al. (2004) and Stuart and Binzel (2004) with some modification. As shown in Table 2, we have seven main taxonomic complexes, namely, A, C, D, Q, S, V, X, whose subdivisions are listed. The main points are that, we combined the R-type into the V-type because they have similar spectral slopes in visible. By the same token, the O-type and the Q-type were merged into the Q-complex. The resultant SEDs of the seven taxonomical groups are illustrated in Fig. 1 which is a composite plot of different types of reflectance spectra to show the range of spectral variations. The actual dispersion should be more than depicted here because the Bus-DeMeo taxonomic classification is based on 371 spectra out of a population of about one million objects. In principle, these curves capture most of the main spectral signatures, namely, the absorption feature near 1 μm for the Q- and V-types, the flatter slopes of X- and C-types, and the reddish color of the A- and D-types. Table 2 also gives the color indices specific to different taxonomic groups.

3.2. Classification

The distribution of the color indices of different taxonomic types is shown in the V-R/B-V color-color diagram in Fig. 2. This figure was constructed by collecting the known color indices of 150 NEAs from the Database of Physical Properties of NEAs by E.A.R.N. (Binzel et al., 2002) and several photometric surveys (Rabinowitz, 1998; Dandy et al., 2003; Ye, 2011). The color indices from the Lulin observations are superimposed over the reference data points. Some of the Lulin data points have relatively large error bars, but most of them fall into the domain of the reference groups aligned by the A-V-S-Q axis and the D-X-C axis.

In order to examine the taxonomic types of the observed NEAs by three color indices, representing different slopes of their SEDs, we adopted the method of principal component analysis (cf. Ivezic et al., 2001) to identify the uncorrelated indices in the B-V and V-R phase space. According to the line of linear regression to the mean indices of the seven taxonomic complexes, we can rotate the B-V and V-R axes by and angle (θ) of 37.43°(with a deviation of +2.714°/-2.937° from the fitting slope of 0.765 ± 0.078) from which we can derive a principal component index (PCI) according to Equation (1).

$$PCI = (B - V)\cos\theta + (V - R)\sin\theta \quad (1)$$

The main method to classify the NEAs is analogous to that of DeMeo and Carry (2013) while using PCI and the R-I index in the present study. Fig. 3.a shows the PCI vs. R-I index of the known taxonomic types. It helps us to identify the boundaries of different complexes according to the Bus-DeMeo system, which described the ranges from the average spectra of the specific classes. Furthermore, we also considered the distributions of previous classifications referred in Fig. 3.a. Fig. 3.b shows the positions of our data points in such a map.

Table 1
Here displays the mean magnitude of each band, color indices, principle component indices (PCI1) and their corresponding deviations of our 92 NEA targets.

NEA	B	ΔB	V	ΔV	R	ΔR	I	ΔI	B-V	ΔB-V	V-R	ΔV-R	V-I	ΔV-I	R-I	ΔR-I	*PCI1*	*ΔPCI1*	
(1036) Ganymed	16.927	0.006	16.045	0.003	15.530	0.004	15.064	0.004	0.882	0.008	0.515	0.004	0.981	0.005	0.466	0.006	1.015	0.009	
(1627) Ivar	13.432	0.008	12.602	0.004	12.170	0.005	11.846	0.005	0.830	0.010	0.432	0.005	0.756	0.005	0.325	0.007	0.924	0.011	
(1685) Toro	17.311	0.056	16.375	0.021	15.886	0.023	15.506	0.024	0.936	0.076	0.489	0.024	0.869	0.027	0.380	0.036	1.043	0.075	
(1943) Anteros	17.140	0.007	16.219	0.004	15.705	0.005	15.243	0.005	0.921	0.009	0.514	0.005	0.976	0.005	0.462	0.007	1.046	0.010	
(2100) Ra-Shalom	17.069	0.010	16.350	0.007	15.901	0.008	15.591	0.013	0.719	0.012	0.449	0.009	0.759	0.017	0.310	0.019	0.845	0.015	
(3360) Syrinx	17.183	0.021	16.355	0.013	15.948	0.013	15.550	0.015	0.828	0.027	0.407	0.013	0.805	0.017	0.398	0.021	0.908	0.029	a
(3554) Amun	18.361	0.027	17.593	0.014	17.202	0.016	16.784	0.016	0.768	0.035	0.391	0.017	0.809	0.018	0.418	0.025	0.850	0.038	
(4055) Magellan	18.978	0.028	18.032	0.016	17.516	0.017	17.275	0.020	0.946	0.036	0.516	0.018	0.757	0.023	0.241	0.029	1.067	0.040	
(4179) Toutatis	15.237	0.019	14.406	0.009	13.941	0.011	13.577	0.011	0.831	0.025	0.465	0.012	0.829	0.013	0.364	0.018	0.945	0.027	
(4450) Pan	18.008	0.023	17.202	0.015	16.733	0.018	16.569	0.025	0.806	0.029	0.469	0.020	0.633	0.032	0.164	0.038	0.927	0.035	
(4487) Pocahontas	18.426	0.038	17.655	0.024	17.166	0.027	16.729	0.030	0.771	0.048	0.489	0.029	0.926	0.035	0.438	0.046	0.911	0.056	a
(4954) Eric	17.651	0.008	16.651	0.004	16.120	0.005	15.707	0.006	1.000	0.010	0.531	0.005	0.944	0.007	0.413	0.009	1.120	0.011	
(5731) Zeus	18.287	0.061	17.578	0.033	17.184	0.038	16.814	0.044	0.709	0.080	0.394	0.042	0.764	0.053	0.369	0.068	0.804	0.089	a
(6047) 1991 TB1	18.863	0.050	18.015	0.033	17.563	0.035	17.244	0.041	0.848	0.062	0.452	0.037	0.771	0.048	0.320	0.061	0.950	0.072	a
(7350) 1993 VA	18.154	0.050	17.337	0.028	16.962	0.033	16.576	0.031	0.817	0.065	0.375	0.037	0.761	0.034	0.384	0.043	0.880	0.074	a
(7753) 1988 XB	16.789	0.029	16.114	0.017	15.742	0.019	15.473	0.021	0.675	0.038	0.372	0.021	0.641	0.025	0.269	0.032	0.764	0.043	a
(8013) Gordonmoore	20.660	0.125	19.831	0.078	19.351	0.083	18.792	0.087	0.829	0.158	0.480	0.087	1.039	0.096	0.559	0.130	0.952	0.179	a
(10115) 1992 SK	18.553	0.046	17.651	0.025	17.208	0.028	16.861	0.028	0.902	0.060	0.443	0.031	0.790	0.031	0.347	0.044	0.988	0.067	a
(11284) Belenus	17.856	0.060	16.985	0.024	16.466	0.025	16.068	0.027	0.871	0.081	0.519	0.025	0.917	0.030	0.398	0.039	1.009	0.080	
(11405) 1999 CV3	17.605	0.057	16.637	0.031	16.126	0.034	15.756	0.035	0.968	0.074	0.511	0.036	0.881	0.038	0.370	0.053	1.082	0.081	a
(12923) Zephyr	19.590	0.102	18.850	0.063	18.320	0.071	17.812	0.079	0.740	0.130	0.530	0.078	1.038	0.092	0.508	0.120	0.910	0.151	a
(17188) 1999 WC2	16.354	0.018	15.636	0.011	15.152	0.014	14.820	0.014	0.718	0.023	0.484	0.017	0.816	0.016	0.374	0.016	0.865	0.029	a
(21088) Chelyabinsk	17.856	0.070	17.166	0.030	16.670	0.034	16.224	0.035	0.690	0.094	0.496	0.037	0.942	0.039	0.446	0.054	0.850	0.098	
(22753) 1998 WT	18.522	0.034	17.763	0.018	17.338	0.020	17.010	0.021	0.759	0.045	0.425	0.021	0.753	0.023	0.328	0.032	0.863	0.049	a
(24761) Ahau	19.095	0.065	18.478	0.039	17.982	0.042	17.518	0.045	0.617	0.084	0.496	0.044	0.960	0.051	0.464	0.067	0.791	0.094	
(25916) 2001 CP44	19.000	0.046	18.123	0.028	17.626	0.030	17.083	0.039	0.877	0.058	0.497	0.032	1.040	0.047	0.543	0.057	1.001	0.066	a
(40267) 1999 GJ4	19.509	0.031	18.641	0.021	18.078	0.022	17.747	0.025	0.868	0.039	0.563	0.023	0.894	0.029	0.331	0.037	1.033	0.045	a
(52762) 1998 MT24	18.310	0.085	17.567	0.058	17.126	0.084	16.758	0.089	0.743	0.106	0.441	0.103	0.809	0.112	0.368	0.016	0.860	0.146	
(53435) 1999 VM40	17.062	0.015	16.160	0.009	15.628	0.010	15.248	0.011	0.902	0.019	0.532	0.011	0.912	0.013	0.381	0.017	1.041	0.022	a
(55532) 2001 WG2	18.572	0.064	17.754	0.037	17.233	0.040	17.062	0.052	0.818	0.082	0.521	0.042	0.692	0.063	0.171	0.076	0.967	0.091	a
(68031) 2000 YK29	18.887	0.019	18.062	0.013	17.561	0.014	17.144	0.016	0.825	0.024	0.501	0.014	0.918	0.018	0.417	0.023	0.961	0.028	a
(68216) 2001 CV26	17.838	0.079	16.875	0.034	16.422	0.036	16.008	0.038	0.963	0.107	0.453	0.037	0.867	0.041	0.414	0.055	1.043	0.108	
(85990) 1999 JV6	19.893	0.058	19.080	0.030	18.729	0.033	18.207	0.038	0.813	0.076	0.351	0.035	0.873	0.045	0.522	0.057	0.862	0.082	a
(88263) 2001 KQ1	18.517	0.037	17.718	0.024	17.371	0.027	16.971	0.032	0.799	0.046	0.347	0.029	0.747	0.038	0.400	0.048	0.849	0.054	a
(89355) 2001 VS78	19.269	0.050	18.403	0.024	17.801	0.026	17.407	0.037	0.866	0.067	0.602	0.028	0.996	0.046	0.394	0.054	1.054	0.071	a
(90075) 2002 VU94	19.166	0.058	18.389	0.032	17.920	0.037	17.447	0.037	0.777	0.076	0.469	0.041	0.942	0.041	0.474	0.058	0.903	0.085	a
(99942) Apophis	16.477	0.019	15.631	0.010	15.180	0.011	14.818	0.012	0.846	0.025	0.451	0.012	0.813	0.013	0.362	0.017	0.948	0.027	
(136900) 1998 HL49	19.683	0.090	18.982	0.061	18.469	0.077	18.112	0.083	0.701	0.111	0.513	0.091	0.870	0.101	0.357	0.136	0.869	0.143	a
(137062) 1998 WM	18.068	0.029	17.208	0.016	16.848	0.018	16.596	0.023	0.860	0.038	0.360	0.019	0.612	0.028	0.252	0.034	0.905	0.042	a
(137199) 1999 KX4	16.667	0.029	15.859	0.014	15.371	0.016	15.042	0.017	0.808	0.038	0.488	0.017	0.817	0.019	0.329	0.026	0.940	0.041	a
(137805) 1999 YK5	17.205	0.031	16.542	0.017	16.127	0.020	15.779	0.021	0.663	0.041	0.415	0.022	0.763	0.024	0.348	0.031	0.780	0.046	
(141052) 2001 XR1	19.269	0.045	18.552	0.031	18.078	0.031	17.728	0.036	0.717	0.055	0.474	0.030	0.824	0.041	0.350	0.051	0.858	0.062	a
(141484) 2002 DB4	17.776	0.046	17.075	0.024	16.636	0.027	16.335	0.026	0.701	0.060	0.439	0.029	0.740	0.027	0.301	0.040	0.825	0.065	a
(152756) 1999 JV3	17.598	0.038	16.591	0.014	16.152	0.016	15.855	0.017	1.007	0.052	0.439	0.018	0.736	0.020	0.297	0.027	1.070	0.052	a
(152889) 2000 CF59	17.894	0.029	17.005	0.013	16.576	0.013	16.354	0.016	0.889	0.039	0.429	0.012	0.651	0.018	0.222	0.021	0.970	0.038	a
(154347) 2002 XK4	17.416	0.040	16.605	0.021	16.132	0.024	15.777	0.024	0.811	0.053	0.473	0.026	0.828	0.026	0.355	0.037	0.933	0.058	a
(162004) 1991 VE	17.213	0.022	16.523	0.019	16.154	0.016	15.740	0.019	0.690	0.024	0.369	0.013	0.783	0.019	0.414	0.023	0.774	0.027	a
(162566) 2000 RJ34	17.196	0.011	16.567	0.007	16.204	0.008	15.843	0.009	0.629	0.014	0.363	0.008	0.724	0.010	0.361	0.013	0.721	0.016	
(163249) 2002 GT	17.457	0.063	16.533	0.026	16.043	0.029	15.741	0.030	0.924	0.085	0.490	0.031	0.792	0.033	0.303	0.045	1.034	0.087	a
(163364) 2002 OD20	15.028	0.029	14.183	0.014	13.747	0.016	13.410	0.017	0.845	0.038	0.436	0.017	0.773	0.020	0.337	0.027	0.939	0.041	a
(168378) 1997 ET30	18.534	0.034	17.681	0.022	17.244	0.024	16.917	0.027	0.853	0.042	0.437	0.026	0.764	0.032	0.327	0.041	0.946	0.049	a
(214869) 2007 PA8	14.635	0.016	13.831	0.009	13.410	0.010	13.097	0.011	0.804	0.020	0.421	0.011	0.734	0.012	0.312	0.016	0.897	0.023	
(215188) 2000 NM	18.364	0.024	17.556	0.012	17.099	0.013	16.727	0.015	0.808	0.031	0.457	0.014	0.829	0.017	0.372	0.022	0.921	0.033	
(219071) 1997 US9	19.761	0.069	18.965	0.049			17.896	0.058	0.796	0.084			1.069	0.066					a

(*continued on next page*)

Table 1 (*continued*)

NEA	B	ΔB	V	ΔV	R	ΔR	I	ΔI	B-V	ΔB-V	V-R	ΔV-R	V-I	ΔV-I	R-I	ΔR-I	*PCI1*	*ΔPCI1*	
(230111) 2001 BE10	18.391	0.109	17.581	0.052	17.196	0.054	16.980	0.060	0.810	0.145	0.385	0.056	0.601	0.067	0.216	0.087	0.880	0.150	
(249595) 1997 GH28	18.226	0.020	17.483	0.013	17.031	0.014	16.590	0.016	0.743	0.025	0.452	0.015	0.893	0.018	0.441	0.023	0.866	0.029	[a]
(249886) 2001 RY11	18.959	0.051	18.312	0.032	17.885	0.034	17.518	0.041	0.647	0.065	0.427	0.036	0.794	0.048	0.324	0.064	0.774	0.074	[a]
(262623) 2006 WY2	18.194	0.024	17.373	0.015			16.477	0.017	0.821	0.031			0.896	0.019					[a]
(276397) 2002 XA40	17.449	0.011	16.628	0.008	16.160	0.010	15.832	0.010	0.821	0.014	0.468	0.011	0.796	0.012	0.333	0.016	0.938	0.018	[a]
(276786) 2004 KD1	19.226	0.057	18.519	0.037	18.203	0.040	17.978	0.054	0.707	0.072	0.316	0.043	0.541	0.066	0.225	0.079	0.756	0.083	[a]
(277127) 2005 GW119	18.948	0.066	18.099	0.038	17.627	0.040	17.310	0.048	0.849	0.086	0.472	0.042	0.789	0.057	0.310	0.071	0.963	0.094	[a]
(285263) 1998 QE2	11.860	0.007	11.127	0.003	10.804	0.005	10.425	0.005	0.733	0.009	0.323	0.007	0.702	0.006	0.380	0.009	0.781	0.011	
(294739) 2008 CM	17.538	0.019	16.791	0.011	16.321	0.012	15.962	0.014	0.747	0.025	0.470	0.012	0.829	0.016	0.359	0.020	0.880	0.027	[a]
(297274) 1996 SK	17.042	0.013	16.275	0.013	15.793	0.013	15.474	0.013	0.767	0.013	0.482	0.013	0.801	0.013	0.320	0.013	0.903	0.018	
(326732) 2003 HB6	17.554	0.094	16.878	0.046	16.490	0.047	16.092	0.050	0.676	0.124	0.388	0.048	0.786	0.054	0.398	0.073	0.774	0.128	[a]
(329338) 2001 JW2	17.319	0.029	16.521	0.016	16.025	0.018	15.637	0.023	0.798	0.037	0.496	0.019	0.884	0.028	0.383	0.034	0.936	0.041	[a]
(330825) 2008 XE3	16.704	0.014	15.870	0.008	15.400	0.009	15.020	0.011	0.834	0.018	0.470	0.009	0.850	0.013	0.380	0.016	0.950	0.020	
(333358) 2001 WN1	17.378	0.030	16.668	0.018	16.230	0.020	15.873	0.024	0.710	0.039	0.438	0.021	0.795	0.029	0.357	0.036	0.831	0.044	
(334412) 2002 EZ2	19.390	0.078	18.590	0.051	18.025	0.060	17.718	0.068	0.800	0.098	0.565	0.068	0.872	0.081	0.308	0.106	0.979	0.119	[a]
(339492) 2005 GQ21	17.387	0.011	16.587	0.007	16.125	0.009	15.746	0.010	0.800	0.014	0.462	0.010	0.841	0.012	0.379	0.016	0.918	0.017	[a]
(339714) 2005 ST1	18.177	0.053	17.323	0.028	16.847	0.032	16.438	0.039	0.854	0.070	0.476	0.036	0.885	0.048	0.409	0.060	0.970	0.078	[a]
(340666) 2006 RO36	19.223	0.032	18.539	0.022	18.135	0.024	17.789	0.029	0.684	0.040	0.404	0.026	0.750	0.034	0.346	0.043	0.790	0.048	[a]
(341816) 2007 YK	19.036	0.112	18.262	0.051	17.833	0.057	17.561	0.046	0.774	0.150	0.429	0.062	0.701	0.040	0.272	0.073	0.877	0.157	[a]
(343098) 2009 DV42	17.391	0.042	16.565	0.022	16.027	0.026	15.584	0.026	0.826	0.055	0.538	0.029	0.981	0.030	0.445	0.043	0.984	0.061	[a]
(345722) 2007 BG29	19.428	0.082	18.438	0.040	17.787	0.043	17.339	0.043	0.990	0.109	0.651	0.046	1.099	0.045	0.448	0.064	1.183	0.115	[a]
(349068) 2006 YT13	16.761	0.034	15.969	0.018	15.503	0.021	15.127	0.021	0.792	0.044	0.466	0.023	0.842	0.024	0.365	0.035	0.914	0.049	
(355256) 2007 KN4	19.557	0.089	18.666	0.054	18.228	0.059	17.814	0.069	0.891	0.113	0.438	0.064	0.852	0.082	0.414	0.105	0.977	0.129	[a]
(356394) 2010 QD2	18.965	0.033	18.080	0.017	17.626	0.019	17.272	0.020	0.885	0.043	0.454	0.020	0.808	0.022	0.354	0.030	0.981	0.046	[a]
(361071) 2006 AO4	17.218	0.032	16.415	0.018	16.038	0.025			0.803	0.041	0.377	0.030					0.870	0.051	[a]
(363790) 2005 JE46	18.442	0.090	17.690	0.051	17.284	0.062	16.974	0.061	0.752	0.117	0.406	0.071	0.716	0.069	0.310	0.100	0.846	0.136	[a]
(378610) 2008 FT6	19.004	0.015	18.092	0.008	17.594	0.009	17.204	0.011	0.912	0.019	0.498	0.010	0.888	0.014	0.390	0.017	1.029	0.021	[a]
(389694) 2011 QD48	19.610	0.049	18.755	0.034	18.249	0.038	17.937	0.045	0.855	0.061	0.506	0.041	0.818	0.053	0.312	0.067	0.988	0.073	[a]
(411280) 2010 SL13	18.171	0.014	17.485	0.009	17.046	0.010	16.627	0.012	0.686	0.018	0.439	0.011	0.858	0.015	0.419	0.019	0.813	0.021	[a]
(441825) 2009 SK1	19.231	0.066	18.558	0.044	18.084	0.048	17.777	0.059	0.673	0.083	0.474	0.051	0.781	0.071	0.308	0.087	0.823	0.097	[a]
2002 TY68	18.445	0.023	17.673	0.016	17.240	0.018	16.835	0.019	0.772	0.029	0.433	0.020	0.838	0.022	0.417	0.031	0.878	0.035	[a]
2005 RQ6	18.674	0.054	17.943	0.028	17.484	0.032	17.162	0.054	0.731	0.071	0.459	0.036	0.781	0.071	0.317	0.059	0.861	0.078	
2010 TN54	18.053	0.061	17.239	0.035	16.804	0.052	16.492	0.053	0.814	0.079	0.435	0.064	0.747	0.066	0.313	0.016	0.913	0.102	[a]
2010 XZ67	16.346	0.004	15.555	0.002			14.791	0.003	0.791	0.006			0.764	0.004					[a]
2011 WV134	16.217	0.011	15.431	0.006	14.990	0.007	14.597	0.008	0.786	0.014	0.441	0.008	0.834	0.009	0.394	0.012	0.894	0.016	
2012 ER14	18.030	0.012	17.424	0.007	17.044	0.008	16.647	0.010	0.606	0.015	0.380	0.009	0.777	0.013	0.397	0.016	0.713	0.017	[a]
2013 SO19	19.968	0.071	19.228	0.050			18.311	0.064	0.740	0.087			0.917	0.075					[a]
2013 UH9	18.520	0.092	17.814	0.052	17.299	0.055	16.865	0.057	0.706	0.119	0.515	0.057	0.949	0.062	0.434	0.084	0.874	0.130	[a]

[a] It indicates that this NEA was derived for its Bessel-system color indices from the photometry for the first time.

Table 2
A list of the seven merged complexes and their subgroups together with the individual color indices.

Taxonomic complex	Subgroups	B-V	V-R	V-I
A	A, Sa	0.926	0.556	0.900
C	C, Cb, Cg, Cgh, Ch, B	0.694	0.365	0.696
D	D, T	0.744	0.444	0.868
Q	Q, Sq, O	0.792	0.444	0.747
S	K, L, Ld, S, Sr, Sv, Sk, Sl	0.818	0.484	0.871
V	V, R	0.861	0.519	0.825
X	X, Xc, Xe, Xk	0.716	0.410	0.785

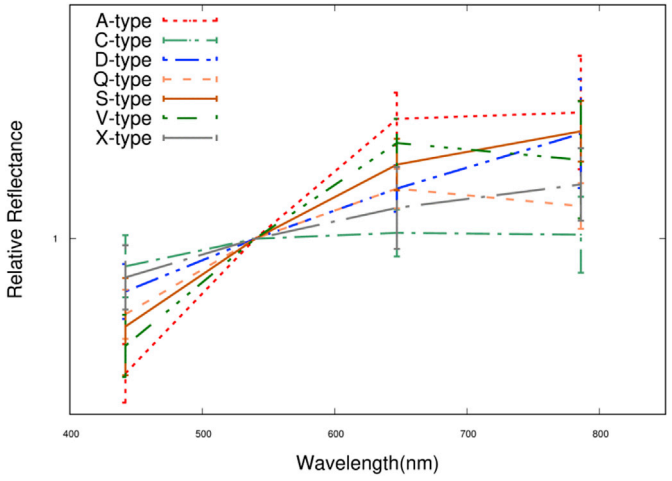

Fig. 1. The relative reflectance spectra of the seven taxonomic complexes. The four conjunct points of 442, 540, 647, and 786 nm correspond to the median wavelengths of the band widths from our BVRI filters. The reflective irradiance is normalized according to the V-band. The error bars are derived from the dispersions of the mean spectra (DeMeo et al., 2009).

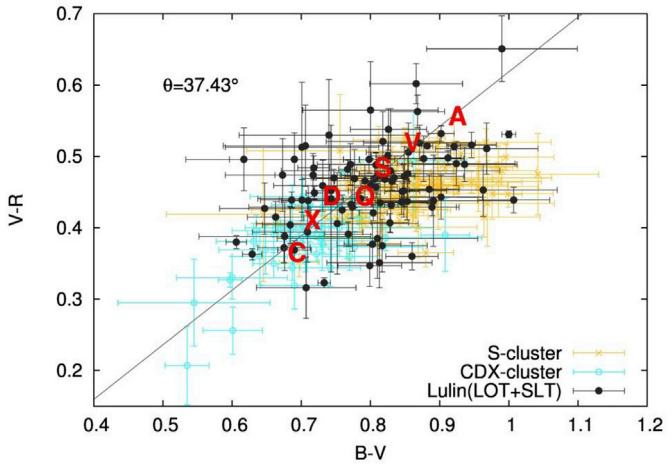

Fig. 2. The color-color diagrams for the spectral indices of the two taxonomic clusters, S- (yellow) and CDX-clusters (blue) (will also be described in Section 5) from the literature and the Lulin observations (black dots). The centers of the mean colors of different spectral complexes are identified with the corresponding red bold letters.

It can be noticed that some of the taxonomic domains overlap with others and that a few of the data points from the Lulin photometric survey fall outside the outer limit of the taxonomic boundaries. The flow chart in

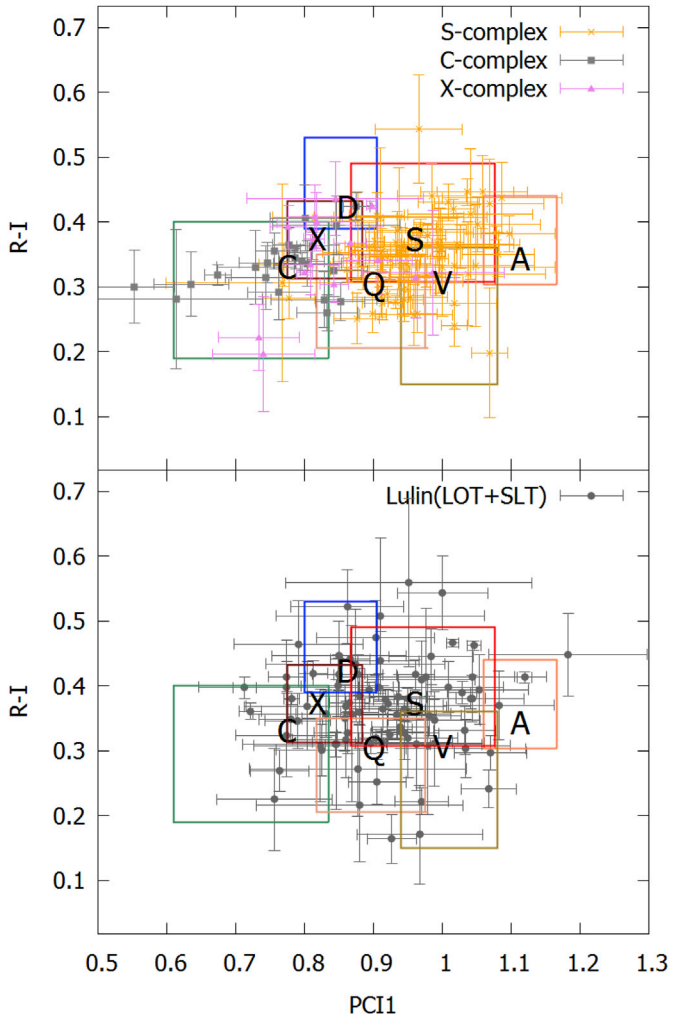

Fig. 3. An illustration of the correlation between the principle-component index (PCI) and the color index, R-I. The black bold letters specify the mean colors of the seven taxonomic complexes, A, C, D, Q, S, V and X. Each has its own domain boundary which is plotted in different colors. (a) Top: The global pattern of the seven domains and the distributions of the three large complexes: C-, S- and X-complexes in the PCI vs. R-I plot. (b) Bottom: Distribution of the 87 NEAs in the same plot.

Fig. 4 illustrates the steps taken to prioritize their identification. Basically, we classified our NEAs according to the boundaries of taxonomic complexes in Fig. 3. Inevitably some photometric classifications would fall into two or more taxonomical regions. If it is really close to the mean indices of one taxonomic complex with the distance of (PCI, R-I) smaller than 0.01, we would classify it to be that one. Otherwise, we have perform priority check as displayed in Fig. 4. The reason is that the Q-complex has a prominent absorption feature, and if one S-complex NEA has some such feature like that, we would consider it as having some Q-type surfaces on it. The majority of the NEA taxonomic classes are inside silicate complexes with a larger amount of V-type than A-type. As for the group of C, D, X-complexes, the X-complex has a higher fraction of overlapping with the regions of C and D complexes and also a larger distinguished population within the CDX-cluster. Therefore, classification of the X-complex has priority.

Five NEAs of the program have only two color indices because of the observational condition. They are classified by visual inspection and comparison of the segmental slopes with the SED templates of the seven

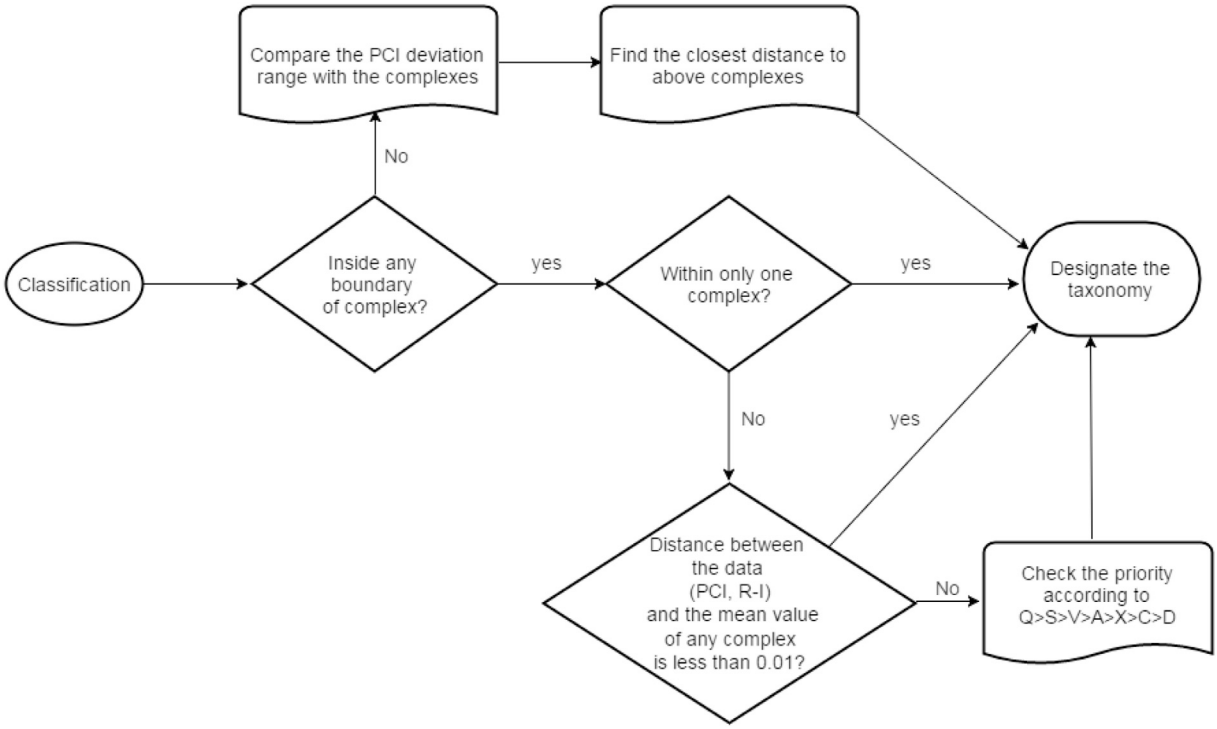

Fig. 4. The flow chart for the classification scheme of NEA taxonomy according to the relative positions of NEAs in Fig. 3.

taxonomic types. The results are listed in Table 3 and Table 4. Note that the sizes of NEAs without albedo measurements have been estimated by using the mean albedos of individual spectral types given in Thomas et al. (2011). Finally, Fig. 5 shows the composite SEDs of the 87 NEAs with full sets of BVRI measurements according to their assigned complexes. The spectra and the descriptions of individual entries can be found in the Appendices.

4. Spectral trends

According to the spectral classifications as described above, it can be seen that there are A = 3%, C = 6.5%, D = 8%, Q = 26%, S = 37%, V = 6.5%, and X = 13% in our Lulin sample (see Fig. 6). In general, such distribution is compatible to the results of Thomas et al. (2011) covering 118 NEAs, with C = 4%, D = 2%, Q = 34%, S = 39%, V = 6%, and X = 15%, but lacking the A-type. The A-complex has similar reddish trend as the S-complex. If we combine A and S together in the Lulin survey, the resultant S-complex will be 40% which is close to the value of Thomas et al. (2011).

It is interesting to see in Fig. 5 that while the spectral classification has been divided into 7 complexes, they could also be grouped into two main clusters, namely, the S-cluster consisting of the S, Q, V and A complexes, and the C-cluster consisting of the C, D and X complexes. The ratio of simply lumped clusters of S and C classes would be more comparable with other results as well as reducing some disadvantage of lower spectral resolution from the photometry. In general, our photometric measurements allow spectral typing according to the Bus-DeMeo system. In our Lulin sample, the S-cluster accounts for nearly 73% of the total number of NEAs and the C-cluster 27%. The corresponding S-cluster to C-cluster (or S/C) ratio is therefore about 2.7. Note that the bias-corrected estimate by Stuart and Binzel (2004) gives a S/C (i.e., bright to dark) ratio of 1.6. Carry et al. (2016) shows the S/C ratio of objects with diameter between 3 and 5 km to be about 2.0 according to SDSS photometric measurements. A larger S/C ratio of 3.3 was reported by Gietzen (2009) based on infrared and other observations.

Furthermore, the overall ratio of C- to C- plus S-cluster of the Lulin samples is 25 over 25 + 67 or 0.27 ± 0.05. The error of the fraction is derived by variance of the beta distribution and will be applied thereafter. The ratio of C-like/S-like is 25/67 or 0.37. This value is larger than the results of previous photometric NEA surveys from Dandy et al. (2003) for 0.21 and Ye (2011) for 0.14, However, it is close to the spectroscopic measurements of 36 NEAs from Lazzarin et al. (2005) for 0.27.

Rabinowitz (1998) suggested that NEAs with $H > 17.0$ and $H < 17.0$, respectively, do not share the same color distributions. Fig. 7 shows the taxonomic distribution divided into two groups of sizes in our Lulin observations. The smaller NEAs with $H > 17.0$ appear to have significantly more C- and D-complex objects. As for the S- and Q-complex objects, the differences are not as obvious. In the Lulin samples, the C-cluster/(C-cluster + S-cluster) ratio of large NEAs with $H \leq 17.0$ is 0.22 ± 0.06, and the smaller ones (with $17.0 < H \leq 22.0$) is 0.31 ± 0.06. This means that the fraction of C-cluster is larger within the smaller NEAs, which have diameters smaller than 1 km using an average albedo of 0.28 (Thomas et al., 2011). Our results show a similar trend as the photometric measurements by Ye (2011) in which the C-like/S-like ratio for H between 18 and 22 is about twice as high as that for $H < 18$, namely, 0.33 vs. 0.17, respectively.

Previous studies by Dandy et al. (2003) and Ye (2011) both supported the hypothesis that smaller NEAs generally have less space weathered surfaces simply because of the lack of regolith. Specifically, the ratio of Q-complex/SQ-group (Q/SQ, hereafter) may be larger for the smaller NEAs. We integrated our Lulin classifications with the previous results for S- and Q-complexes (Binzel et al., 2002: Data Base of Physical and Dynamical Properties of NEAs on E.A.R.N.) and divided the population close to 600 NEAs into two groups according to H, relevant to their sizes. The ratio of Q/SQ for $H > 17.0$ is 0.45 ± 0.03, as to that for $H \leq 17.0$ is

Table 3
Physical properties of the NEAs in the Lulin sample which have been taxonomically identified before.

NEA	a(AU)	e	i(∘)	q(AU)	H	albedo	D(km)	T_J [a]	Pre. tax. by spectroscopy	Pre. tax. by photometry	Taxonomy in this work
(1036) Ganymed	2.663	0.534	26.692	1.241	9.45	0.228	36.49	3.03	S	S	S
(1627) Ivar	1.863	0.396	8.451	1.124	13.2	0.134	8.37	3.88	S	S	Q
(1685) Toro	1.367	0.436	9.381	0.771	14.23	0.26	3.75	4.72	S	S	S
(1943) Anteros	1.430	0.256	8.706	1.064	15.75	0.17	2.48	4.64	S; L;Sw		S
(2100) Ra-Shalom	0.832	0.437	15.758	0.469	16.05	0.14	2.24	6.95	K; Sr; C		Q
(3554) Amun	0.974	0.280	23.362	0.701	15.82	0.142	3.34	6.11	X; M;D		X
(4055) Magellan	1.820	0.327	23.257	1.226	14.6	0.33	2.781	3.89	V		V
(4179) Toutatis	2.534	0.629	0.447	0.939	15.3	0.13	4.3	3.14	S; Sk		S
(4450) Pan	1.442	0.586	5.520	0.596	17.1		0.9–1.1[b]	4.46	S/Sr	S	Q
(4954) Eric	2.002	0.449	17.446	1.104	12.6	mh	9.5	3.66	S	S	A
(6047) 1991 TB1	1.454	0.352	23.473	0.942	17.8	0.8	1.2	4.49	S		Q
(7350) 1993 VA	1.356	0.391	7.262	0.826	17	0.05	2.363	4.77	C; X		X
(7753) 1988 XB	1.468	0.482	3.123	0.760	18.6	d	1	4.47	B		C
(8013) Gordonmoore	2.199	0.432	7.571	1.249	16.9	m	1.2	3.53	Sr		S
(10115) 1992 SK	1.248	0.325	15.322	0.843	17	0.28	1	5.06	S:; Sq		S
(11284) Belenus	1.740	0.337	1.993	1.153	18.1		0.58–0.67[b]	4.08		S	S
(11405) 1999 CV3	1.460	0.394	22.863	0.885	15.2	m	3.4	4.46	Sq		A
(12923) Zephyr	1.962	0.492	5.304	0.997	15.8	0.176	2.06	3.72	S		S
(21088) Chelyabinsk	1.707	0.239	38.461	1.299	14.2	0.179	4.23	3.92	Sl; Q	S	D/S
(22753) 1998 WT	1.219	0.570	3.207	0.524	17.7	0.27	0.9	5.06	Q; Sq		Q
(24761) Ahau	1.335	0.306	21.921	0.927	17.3		2.3–4.6[b]	4.79	CX	S	D
(25916) 2001 CP44	2.560	0.498	15.749	1.284	13.6	0.262	5.683	3.20	Q,Sq		S
(40267) 1999 GJ4	1.339	0.808	34.529	0.257	15.4	0.249	1.62	4.38	Sq		S
(52762) 1998 MT24	2.418	0.651	33.894	0.843	14.8	0.052	6.71	3.01		X	X
(53435) 1999 VM40	2.309	0.485	15.388	1.188	14.7	mh	3.8	3.38	S; Srw		S
(55532) 2001 WG2	1.795	0.696	38.500	0.546	16.1	0.14	1.96	3.56	Sk		V
(68216) 2001 CV26	1.319	0.326	17.997	0.889	16.4	0.29	1.4	4.85	Sq	R	S
(85990) 1999 JV6	1.007	0.311	5.326	0.694	20.1	0.095	0.451	6.00	Xk		D
(89355) 2001 VS78	1.787	0.308	22.666	1.236	15.6	0.18	2.3	3.94	S; Sr		S
(99942) Apophis	0.922	0.191	3.331	0.746	19.2	0.3	0.375	6.47	Sq,Scom		S
(137062) 1998 WM	1.225	0.315	22.516	0.838	16.6	0.284	1.265	5.10	Q; Sq		Q
(137199) 1999 KX4	1.457	0.293	16.570	1.031	16.9		1.0–1.2[b]	4.54	Sq		Q
(137805) 1999 YK5	0.829	0.558	16.742	0.366	16.6	0.027	3.879	6.91	X	RQ	X
(141052) 2001 XR1	1.246	0.550	17.659	0.560	17.3	0.22	1	4.96	Sq		Q
(141484) 2002 DB4	0.858	0.370	16.603	0.541	16.4		1.2–1.5[b]	6.79	S; S-		Q
(152756) 1999 JV3	1.451	0.415	15.223	0.848	18.9	mh	0.5	4.51	Sa; S		V
(154347) 2002 XK4	1.850	0.692	17.806	0.570	16		1.5–1.75[b]	3.63	S-		S
(162566) 2000 RJ34	2.635	0.574	13.861	1.121	15.7	0.07	4.41	3.11		X	C
(163249) 2002 GT	1.344	0.335	6.967	0.894	18.4		0.37–0.5[b]	4.82	Sq		V
(163364) 2002 OD20	1.366	0.369	4.188	0.862	18.8		0.4–0.5[b]	4.76	Sq		Q
(214869) 2007 PA8	2.824	0.662	1.984	0.955	16.3	0.29	1.9	2.95	Q; S	Xc	Q
(215188) 2000 NM	2.690	0.663	22.357	0.907	15.4	m	2.6	2.93	Sr	R	S/A
(219071) 1997 US9	1.053	0.282	20.017	0.756	17.1	0.35	1.2	5.75	Q; S		S
(230111) 2001 BE10	0.823	0.369	17.510	0.519	19.1	0.253	0.4	7.03	Scomp	R	Q
(277127) 2005 GW119	1.641	0.233	2.882	1.258	18.7		0.43–0.52[b]	4.26	Sq		Q
(285263) 1998 QE2	2.423	0.572	12.857	1.038	17.3	0.06	2.75	3.24	Ch	Ch	C
(297274) 1996 SK	2.434	0.795	1.964	0.500	16.7		1.09–1.3[b]	2.97		S	Q
(330825) 2008 XE3	2.607	0.550	7.476	1.172	16.3		1.33–1.52[b]	3.17		S	S
(333358) 2001 WN1	1.502	0.303	14.070	1.047	19.5		0.19–1.18[b]	4.46		C	X
(349068) 2006 YT13	1.323	0.426	38.243	0.760	18.3		0.53–0.61[b]	4.65		AR	S
(363790) 2005 JE46	1.903	0.553	8.264	0.851	17.7		0.69–0.82[b]	3.73	C/X/T		Q
2005 RQ6	2.504	0.551	12.484	1.124	18.9		0.40–0.47[b]	3.21	S/Sr		Q
2011 WV134	2.784	0.679	6.047	0.893	17.2		0.88–1.01[b]	2.94		S	S

[a] The Jovian Tisserand parameters.
[b] Note that the sizes are estimated by using the mean albedos of different spectral types of the NEAs according to Thomas et al. (2011).

0.34 ± 0.03, greater than the former one. It indicates that the proportion of Q-complex, namely, those with relatively younger surface occupies more within the smaller NEAs. It is consistent with the surveys as mentioned above.

5. Discussion and summary

Photometric observations of NEAs carried out at the Lulin observatory between 2012 and 2014 have produced BVRI color indices of 92 NEAs. These NEA samples cover the largest NEA, 1036 Ganymed, with a diameter of 35 km to sub-kilometer sized objects with diameter as small as 200 m. The main results are as follows.

(1) The spectral types of the 92 NEAs can be classified into seven merged spectral groups: A, C, D, Q, S, V and X complexes.
(2) Sixty four of the NEAs observed in the present survey are provided with newly identified colors representing 40% increase of the present database of the Bessel-system color indices, as to thirty nine of them present 5% increase to the number of NEAs with classified taxonomic types.
(3) The fractional abundances of seven spectral complexes in this work can be summarized as: A = 3%, C = 6.5%, D = 8%, Q = 26%,

Table 4
Physical properties of the NEAs in the Lulin sample which have new taxonomic identifications.

NEA	a(AU)	e	i	q(AU)	H	albedo	D(km)	T_J [a]	Taxonomy in this work
(3360) Syrinx	2.468	0.746	21.153	0.628	15.9	0.07	1.8	2.96	D
(4487) Pocahontas	1.730	0.296	16.403	1.217	17.4		0.8–0.92[b]	4.06	S
(5731) Zeus	2.263	0.654	11.428	0.784	15.7	0.031	5.231	3.28	X
(17188) 1999 WC2	2.216	0.637	29.444	0.805	16.5	0.147	1.819	3.22	S
(68031) 2000 YK29	1.376	0.129	15.173	1.199	18.1		0.58–0.67[b]	4.77	S
(88263) 2001 KQ1	2.097	0.432	38.819	1.191	15.4	0.048	5.31	3.37	X
(90075) 2002 VU94	2.133	0.576	8.916	0.905	15.2	0.197	2.857	3.47	S
(136900) 1998 HL49	1.747	0.636	11.000	0.635	17.3		0.84–0.96[b]	3.86	S
(152889) 2000 CF59	1.679	0.640	41.590	0.604	16.5	0.388	1.022	3.75	Q
(162004) 1991 VE	0.891	0.665	7.221	0.299	18.2		0.35–2.15[b]	6.46	X
(168378) 1997 ET30	2.138	0.449	6.812	1.179	16.8		1.04–1.24[b]	3.57	Q
(249595) 1997 GH28	2.004	0.371	7.014	1.260	17.7		1.92–3.83[b]	3.74	D
(249886) 2001 RY11	1.483	0.283	22.846	1.063	17.4		1.01–1.56[b]	4.45	C
(262623) 2006 WY2	0.983	0.333	27.554	0.656	18.6	0.122	0.761	6.02	S
(276397) 2002 XA40	2.263	0.482	4.453	1.172	17.1		0.91–1.08[b]	3.45	Q
(276786) 2004 KD1	1.720	0.330	10.124	1.152	17.7		0.88–1.36[b]	4.09	C
(294739) 2008 CM	1.567	0.408	35.998	0.927	17.3		0.84–0.96[b]	4.13	S
(326732) 2003 HB6	2.718	0.572	6.594	1.164	17.6		0.46–2.84[b]	3.09	X
(329338) 2001 JW2	1.698	0.489	9.586	0.868	19.1		0.36–0.42[b]	4.05	S
(334412) 2002 EZ2	1.249	0.046	13.025	1.192	20.1	0.4	0.21	5.12	V
(339492) 2005 GQ21	1.426	0.215	47.024	1.119	18.2		0.56–0.64[b]	4.35	S
(339714) 2005 ST1	1.451	0.371	20.234	0.913	20.4		0.20–0.23[b]	4.51	S
(340666) 2006 RO36	0.906	0.231	23.857	0.697	17.8		0.42–2.59[b]	6.49	X
(341816) 2007 YK	1.870	0.321	31.838	1.269	17.5		0.76–0.90[b]	3.75	Q
(343098) 2009 DV42	1.615	0.275	19.926	1.170	18.7		0.44–0.50[b]	4.23	S
(345722) 2007 BG29	0.833	0.335	18.511	0.554	18	0.258	0.653	6.97	A
(355256) 2007 KN4	3.342	0.630	12.538	1.235	16.8		1.06–1.21[b]	2.77	S/D
(356394) 2010 QD2	2.010	0.785	10.639	0.431	17.4		0.80–0.92[b]	3.35	S
(361071) 2006 AO4	2.629	0.584	24.392	1.095	15.4		1.98–2.36[b]	3.03	Q
(378610) 2008 FT6	2.138	0.426	13.585	1.228	17.4		0.80–0.92[b]	3.56	S
(389694) 2011 QD48	1.545	0.492	19.067	0.785	18.2		0.41–0.55[b]	4.26	V
(411280) 2010 SL13	2.005	0.415	3.041	1.173	19.3		0.21–1.30[b]	3.72	X
(441825) 2009 SK1	1.611	0.223	30.818	1.252	18.3		0.52–0.62[b]	4.16	Q
2002 TY68	2.217	0.514	20.800	1.077	18.7		1.21–2.42[b]	3.39	D
2010 TN54	2.110	0.445	4.721	1.172	19.2		0.35–0.41[b]	3.60	Q
2010 XZ67	2.061	0.494	11.841	1.042	19.7		0.27–0.33[b]	3.60	Q/V
2012 ER14	1.637	0.363	6.863	1.042	20.5		0.24–0.37[b]	4.22	C
2013 SO19	2.228	0.498	12.936	1.118	21.8		0.07–0.41[b]	3.44	X/D
2013 UH9	2.580	0.597	13.075	1.039	18.6		1.27–2.53[b]	3.12	D

[a] The Jovian Tisserand parameters.
[b] Note that the sizes are estimated by using the mean albedos of different spectral types of the NEAs according to Thomas et al. (2011).

S = 37%, V = 6.5%, and X = 13%. This distribution is in agreement with the results of Thomas et al. (2011).

(4) The ratios of C- cluster to itself plus S- cluster are 0.22 ± 0.06 for $H \leq 17.0$ and 0.31 ± 0.06 for $H > 17.0$, respectively, indicating a slightly higher fraction of dark-object population in sub-kilometer size range.
(5) There is also an interesting S-complex target, (355256) 2007 KN4 with Tisserand parameter (T_J) = 2.77 that needs to be investigated further to see if it is a candidate object of cometary origin.
(6) The sizes of the observed NEAs are estimated using either published albedo values or the mean albedos specific to individual taxonomic types.

There are still some anomalous SED curves among our NEAs. For example, the NEA 12923, 24761, 85990, 136900, 441825 etc. have unusual slopes in their reflectance spectra (see Appendix B). It is possibly due to the effect of rotation since the surface spectra of NEAs might have large variations (Lin et al., 2014) and many of them have fast spin rates. As mentioned in Section 2, there were only 31 targets applied with the exposure sequence of RBRVRIR. And we additionally conducted interpolation method to avoid the color deviation from the rotation for this small group within our targets. We also compared the colors both with and without interpolation and found that there are differences of color indices merely less than 2% for these 31 NEAs. However, it is possible that these targets were observed in short exposure time (total time of single sequence < 10 min). If the NEAs were observed over long durations of exposure time (total time of single sequence > 10 min) and only had simple filter sequence of BVRI, it might cause larger deviations of the color measurements. Thus, it would lead to the deformed spectra and subsequently misguide our classifications.

While most of the results of Thomas et al. (2011) and our present work are in very good agreement, the D- and Q-complexes somehow show noticeable differences (Fig. 6). The D-complex difference could be a matter of small number statistics in the Lulin sample. The Q-complex difference is significant and needs to be checked by collecting a large photometric data set in future.

Compared with the previous classifications of the individual NEAs (Appendix C), we assume that there are 3 mis-distinguished targets of each taxonomic complex in average. Hence we can generally added an uncertainty to each fractional abundance of our spectral complexes: $A = 3 \pm 3\%$, $C = 6.5 \pm 3\%$, $D = 8 \pm 3\%$, $Q = 26 \pm 3\%$, $S = 37 \pm 3\%$, $V = 6.5 \pm 3\%$, and $X = 13 \pm 3\%$.

In order to find the difference of bias between our and others' taxonomic distribution during the same observing years, we collected many results of taxonomic detection from late 2011 to the end of 2014 as possible. The results were derived from both spectrometric and photometric observations (Polishook et al., 2014; Lim et al., 2012; Godunova et al., 2013; Ieva et al., 2014; Popescu et al., 2014; Kuroda et al., 2014;

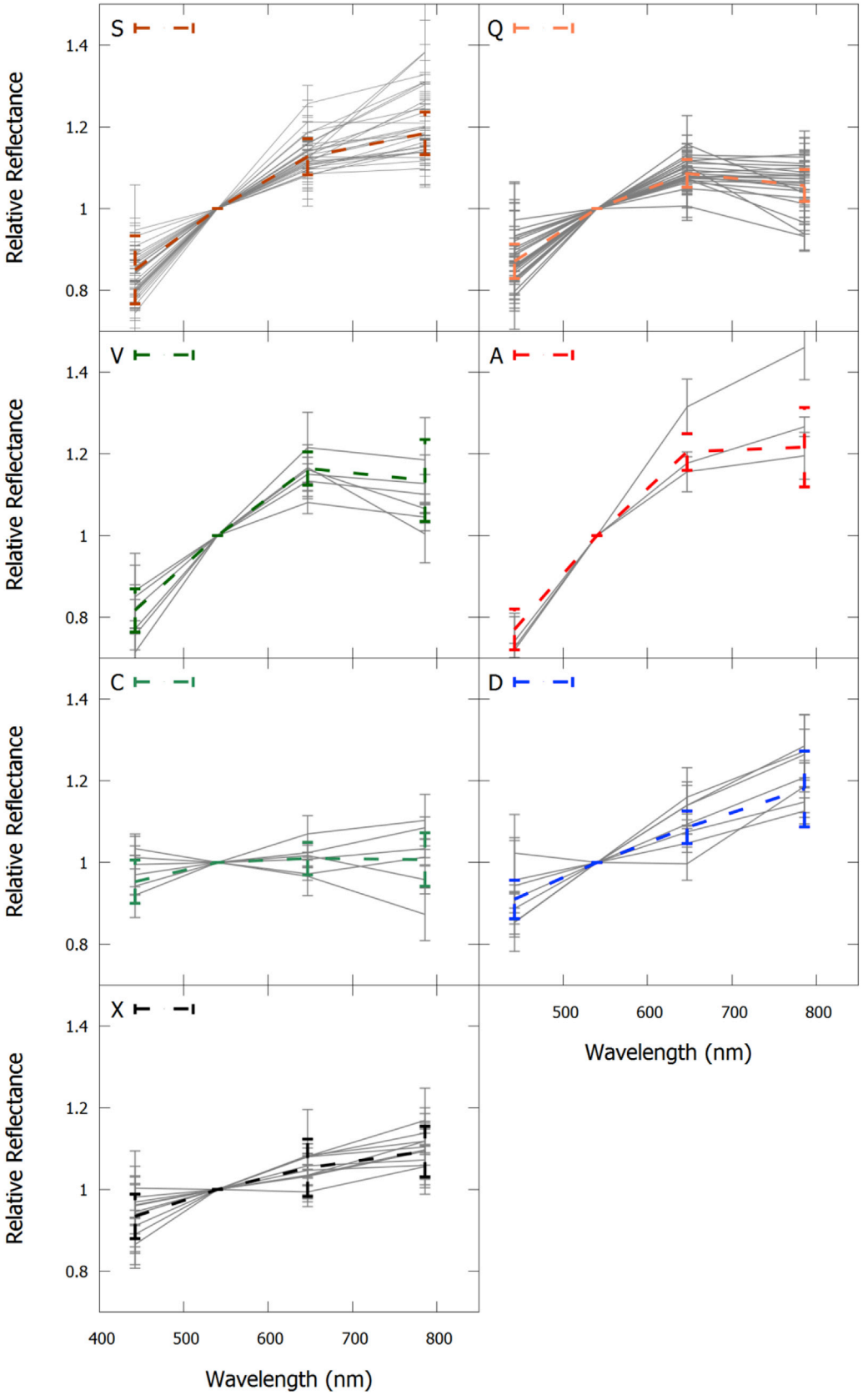

Fig. 5. The composite diagrams of the classified NEA spectra in the 7 taxonomic complexes with the templates of the relative reflectance spectra used in this work.

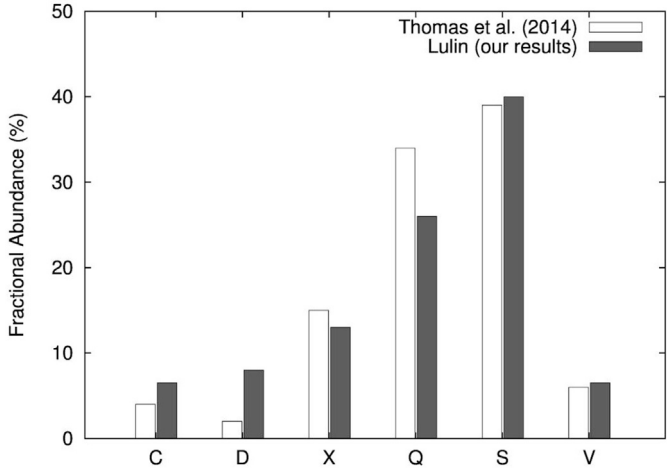

Fig. 6. The fractional abundances of the taxonomic complexes classified within the Lulin samples of 92 NEAs as well as the comparable results of Thomas et al. (2014). The three largest groups in order are S (37%), Q (26%) and X (13%).

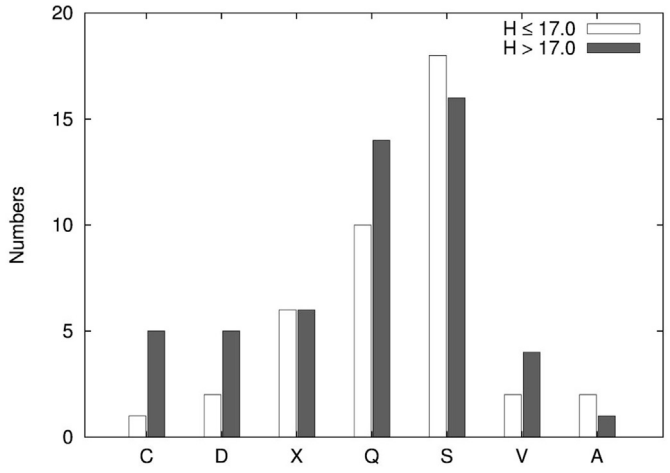

Fig. 7. The numbers of NEAs in different spectral complexes according to their sizes in terms of magnitudes $H \leq 17.0$ and $H > 17.0$, respectively.

Tubiana et al., 2015; Perna et al., 2016; Hicks' Atel. in 2011–2014 (Hicks and Dombroski, 2012; Hicks et al., 2011, 2012a,2012b, 2012c, 2012d, 2012e, 2012f, 2012g, 2012h, 2013a, 2013b, 2013c, 2013d,2013e, 2014a, 2014b; Hicks and Ebelhar, 2013a, 2013b, 2014a, 2014b); Rayner et al., 2003: The MIT-UH-IRTF Joint Campaign for NEO Spectral Reconnaissance). There are total 80 NEAs of targets and some of them are overlapping with ours. Their spectral classifications are also issued into the seven complexes we described above. Thus, the fractional abundances of these external results are of S = 35%, Q = 35%, A = 1%, V = 5%, C = 15%, D = 1%, X = 8%. The ratio of lumped S-/C-cluster is about 3.2, kind of higher than ours (2.7). The distribution of Q, C, D and X complexes are also distinct from our fractions. Certainly there are biases existing in both our and these results since the estimated S/C ratio of debias distribution of NEAs from Stuart and Binzel (2004) is lower (1.6). Note that our spectral distribution is not debiased and the bias might be coming from the target selection, detecting limit of the various instruments and undetected dark population etc. In addition, we integrated our results with the above ones, and then the total fractional abundances would become S = 36%, Q = 30%, A = 2%, V = 6%, C = 10.5%, D = 5%, X = 10.5%. These fractions might be a little more reliable because of larger sample numbers.

Our present study together with the previous work by Ye (2011) showed that photometric measurements at Lulin Observatory can provide very useful taxonomic classifications of NEAs. Even though the color ratios for the relative reflectance spectra are not able to classify the spectral types of the asteroids more specifically and some mis-classification may occur, the simpler taxonomic complexes described in this paper are still generally distinguishable. In future work, we will organize more efficient scheme for observations and data analysis. A topic we will investigate is the correlation of the orbital parameters with the shapes and rotation periods of NEAs in different spectral types. Some interesting insight on their origin and dynamical evolution might be revealed by such statistical study.

Acknowledgments

This work was mainly supported by the Project 017/2014/A1 of Macau Science and Technology Development Fund: MSAR No. 0426 as well as the Lulin Observatory which is operated by Institute of Astronomy, National Central University, Taiwan, under MOST grant: MOST 104-2119-M-008-024. We specially acknowledge that the Lulin staff, Hung-Chin Lin, Chi-Sheng Lin and Hsiang-Yao Hsiao have provided assistance in observations; also the partial support from the open project (No. OP201306) of Key Laboratory for the Structure and Evolution of Celestial Objects, Chinese Academy of Sciences.

Appendix A. Supplementary data

Supplementary data related to this article can be found at https://doi.org/10.1016/j.pss.2017.12.019.

Appendices.

A. The observation log
B. The figure panels of relative reflectance spectra of 87 NEAs
C. The elaborations of observation results for individual NEAs in this paper

A. Observation log

Here displays the observation log of this work. Some targets were observed more than one night. If there are two exposure times (Exp. Time) in a row, the first quantity is for B-filter and the second is for V, R, I.

Designation	Δ (A.U.)[i]	r (A.U.)[ii]	El. (°)[iii]	Ph. (°)[iv]	Observed Date	Vobs	Exp. Time	BVRI sets[v]	Telescope
(1036) Ganymed	3.817	4.062	97.3	13.9	2014 Jan. 9	16.1	180s, 150s	1	LOT
(1627) Ivar	0.378	1.181	107.1	55.1	2013 May 31	13.0	30s	2	SLT
	0.322	1.123	101.0	62.7	2013 Jul. 7	12.4	60s	3	SLT
(1685) Toro	0.991	1.496	98.4	40.6	2013 Jan. 27	16.3	90s	1	LOT
	0.982	1.508	100.1	40.0	2013 Jan. 29	16.4	60s	1	LOT
(1943) Anteros	0.515	1.434	144.5	23.4	2014 Jan. 9	16.2	180s, 150s	1	LOT
(2100) Ra-Shalom	0.348	1.129	101.7	60.8	2013 Sep. 14	16.4	90s, 60s	1	LOT
(3360) Syrinx	0.540	1.510	161.1	12.3	2012 Nov. 13	16.4	30s	1	LOT
(3554) Amun	0.743	1.235	90.1	52.9	2013 Jan. 29	17.6	180s	1	LOT
(4055) Magellan	1.388	2.280	147.5	13.4	2014 Jan. 9	18.0	270s, 240s	1	LOT
(4179) Toutatis	0.298	1.271	162.0	13.9	2013 Jan. 18	14.4	60s	3	SLT
(4450) Pan	0.364	1.304	139.3	30.2	2013 Sep. 14	17.2	90s, 60s	1	LOT
(4487) Pocahontas	0.354	1.221	121.5	44.2	2012 Oct. 9	17.5	60s	2	LOT
	0.358	1.219	120.6	44.8	2012 Oct. 12	17.6	60s	6	LOT
	0.360	1.219	120.2	45.0	2012 Oct. 13	17.6	60s	6	LOT
	0.469	1.233	110.2	48.8	2012 Nov. 13	18.3	60s	2	LOT
(4954) Eric	1.546	1.926	96.6	30.5	2014 Jan. 11	16.7	180s, 150s	1	LOT
(5731) Zeus	0.706	1.346	102.9	46.3	2012 Oct. 9	17.7	45s	3	LOT
	0.416	1.009	80.6	75.4	2012 Nov. 13	17.4	30s	3	LOT
(6047) 1991 TB1	0.476	1.405	142.1	25.9	2012 Oct. 9	18.0	60s	2	LOT
(7350) 1993 VA	0.322	1.054	90.9	71.4	2012 Oct. 9	17.3	45s	2	LOT
(7753) 1988 XB	0.272	1.284	173.3	5.2	2013 May 31	16.1	240s	3	SLT
(8013) Gordonmoore	1.091	2.006	147.1	15.7	2013 Oct. 5	19.6	300s, 240s	1	LOT
	1.125	2.022	144.2	16.8	2013 Oct. 8	19.9	360s, 300s	2	LOT
(10115) 1992 SK	0.419	1.154	103.0	56.3	2013 Jan. 29	17.7	180s	3	LOT
(11284) Belenus	0.248	1.163	131.3	39.5	2013 Jan. 28	17.0	60s	1	LOT
(11405) 1999 CV3	0.661	1.556	141.2	23.4	2013 Jan. 29	16.6	60s	2	LOT
(12923) Zephyr	1.266	1.684	95.2	36.3	2013 Oct. 3	18.9	300s, 240s	1	LOT
	1.192	1.797	110.1	31.4	2013 Oct. 20	18.8	300s, 240s	1	LOT
(17188) 1999 WC2	0.324	1.299	146.6	25.6	2013 Jul. 7	15.6	180s	3	SLT
(21088) Chelyabinsk	1.145	1.309	74.3	48.3	2013 May 31	17.2	300s	1	SLT
(22753) 1998 WT	0.547	1.529	172.4	4.9	2013 Jan. 30	17.8	180s	3	LOT
(24761) Ahau	0.401	1.046	87.3	70.2	2013 Jan. 30	18.5	180s	2	LOT
(25916) 2001 CP44	2.207	2.023	66.3	26.4	2014 Jan. 12	18.1	270s, 240s	1	LOT
(40267) 1999 GJ4	0.981	1.537	103.0	38.6	2014 Jan. 11	18.6	270s, 240s	1	LOT
(52762) 1998 MT24	1.251	2.172	147.7	14.4	2013 Sep. 1	17.6	300s	2	SLT
(53435) 1999 VM40	0.660	1.219	91.7	55.5	2013 Sep. 14	16.5	90s, 60s	1	LOT
	0.638	1.528	139.8	24.6	2014 Jan. 9	15.8	180s, 150s	1	LOT
(55532) 2001 WG2	0.710	1.499	123.7	33.1	2014 Jan. 11	17.8	180s, 150s	1	LOT
(68031) 2000 YK29	0.363	1.221	123.2	42.4	2014 Jan. 9	18.0	270s, 240s	1	LOT
(68216) 2001 CV26	0.353	1.066	93.5	67.2	2013 Jan. 27	16.9	60s	1	LOT
	0.351	1.076	95.3	65.7	2013 Jan. 29	16.9	60s	1	LOT
(85990) 1999 JV6	0.150	1.057	115.8	56.9	2014 Jan. 9	19.0	270s, 240s	1	LOT
(88263) 2001 KQ1	0.838	1.425	101.4	43.4	2012 Oct. 9	17.7	60s	1	LOT
(89355) 2001 VS78	0.893	1.284	86.2	49.8	2014 Jan. 12	18.4	270s, 240s	1	LOT
(90075) 2002 VU94	1.193	1.619	95.7	37.2	2014 Jan. 9	18.1	270s, 240s	1	LOT
	1.162	1.603	96.4	37.6	2014 Jan. 11	18.6	270s, 240s	1	LOT
(99942) Apophis	0.100	1.062	139.9	36.7	2013 Jan. 18	15.8	180s	3	SLT
	0.113	1.079	144.8	31.7	2013 Jan. 29	15.7	60s	3	LOT
	0.115	1.081	144.6	31.9	2013 Jan. 30	15.4	60s	2	LOT
(136900) 1998 HL49	0.688	1.109	80.1	62.2	2013 Oct. 20	19.0	300s, 240s	1	LOT
(137062) 1998 WM	0.446	1.197	107.6	51.5	2014 Jan. 12	17.2	180s, 150s	1	LOT
(137199) 1999 KX4	0.224	1.145	131.6	40.0	2013 Jan. 18	15.9	120s	3	SLT
	0.285	1.226	133.1	37.2	2013 May 31	15.9	240s	1	SLT
(137805) 1999 YK5	0.333	1.134	108.3	55.5	2013 Jan. 18	16.5	240s	4	SLT
(141052) 2001 XR1	0.646	1.509	131.5	29.8	2013 Oct. 2	18.6	210s, 180s	1	LOT
	0.680	1.559	135.7	26.6	2013 Oct. 10	18.6	300s, 240s	1	LOT
(141484) 2002 DB4	0.372	0.934	71.4	86.4	2014 Jan. 11	17.1	180s, 150s	2	LOT
(152756) 1999 JV3	0.146	1.109	127.5	46.6	2013 May 31	16.6	300s	1	SLT
(152889) 2000 CF59	0.487	1.317	123.2	38.8	2013 Jan. 30	17.0	180s	2	LOT
(154347) 2002 XK4	0.523	1.460	149.7	19.9	2013 Jan. 18	16.4	240s	3	SLT
	0.644	1.573	149.3	18.7	2013 Jan. 29	17.1	120s	1	LOT
(162004) 1991 VE	0.223	1.191	152.0	22.9	2012 Nov. 13	16.5	30s	2	LOT
(162566) 2000 RJ34	0.435	1.153	101.6	56.7	2014 Jan. 11	16.6	180s, 150s	1	LOT
(163249) 2002 GT	0.179	1.158	140.7	33.7	2013 May 31	16.5	240s	3	SLT
(163364) 2002 OD20	0.062	1.068	150.0	28.3	2013 May 31	14.2	30s	5	SLT
(168378) 1997 ET30	0.655	1.646	168.9	6.7	2013 Oct. 9	17.8	240s, 180s	1	LOT

(*continued on next page*)

(*continued*)

Designation	Δ (A.U.)[i]	r (A.U.)[ii]	El. (°)[iii]	Ph. (°)[iv]	Observed Date	Vobs	Exp. Time	BVRI sets[v]	Telescope
	0.663	1.652	167.7	7.4	2013 Oct. 10	17.6	240s, 180s	1	LOT
(214869) 2007 PA8	0.185	1.181	169.3	9.0	2012 Oct. 9	13.7	30s	7	LOT
	0.362	1.187	115.8	48.3	2013 Jan. 18	16.4	240s	2	SLT
	0.393	1.268	128.6	37.4	2013 Jan. 28	16.4	90s	2	LOT
(215188) 2000 NM	1.019	1.274	79.0	49.3	2014 Jan. 11	17.6	270s, 240s	1	LOT
(219071) 1997 US9	0.665	1.168	86.6	58.8	2013 Oct. 2	19.0	210s, 180s	1	LOT
(230111) 2001 BE10	0.193	1.111	126.6	45.4	2013 Jan. 28	17.6	180s	1	LOT
(249595) 1997 GH28	0.363	1.277	138.3	30.8	2014 Jan. 9	17.8	180s, 150s	2	LOT
	0.360	1.280	139.9	29.7	2014 Jan. 11	17.4	180s, 150s	1	LOT
	0.359	1.282	140.7	29.1	2014 Jan. 12	16.9	180s, 150s	1	LOT
(249886) 2001 RY11	0.640	1.612	165.1	9.0	2013 Jan. 30	18.3	180s	3	LOT
(262623) 2006 WY2	0.279	1.247	158.3	16.9	2014 Jan. 9	17.4	180s, 150s	1	LOT
(276397) 2002 XA40	0.293	1.173	120.2	47.3	2012 Oct. 12	16.6	60s	5	LOT
	0.294	1.173	120.2	47.3	2012 Oct. 13	16.6	60s	4	LOT
(276786) 2004 KD1	0.575	1.532	151.9	17.9	2013 Oct. 2	18.5	210s, 180s	1	LOT
	0.610	1.569	153.6	16.4	2013 Oct. 10	18.5	300s, 240s	1	LOT
(277127) 2005 GW119	0.287	1.258	156.5	18.3	2012 Nov. 13	18.1	45s	4	LOT
(285263) 1998 QE2	0.039	1.049	153.3	25.7	2013 May 31	11.6	20s	6	SLT
	0.039	1.051	158.7	20.5	2013 Jun. 1	11.4	10s	13	SLT
(294739) 2008 CM	0.222	1.026	94.8	72.8	2014 Jan. 11	16.8	180s, 150s	1	LOT
(297274) 1996 SK	0.443	1.454	173.9	4.2	2012 May 22	16.2	60s	6	LOT
	0.456	1.467	172.8	5.0	2012 May 23	16.5	60s	1	LOT
(326732) 2003 HB6	0.272	1.211	130.6	39.6	2012 July 5	16.9	60s	3	LOT
(329338) 2001 JW2	0.165	1.139	153.0	23.2	2012 Nov. 13	16.5	30s	5	LOT
(330825) 2008 XE3	0.292	1.221	134.8	35.4	2012 Oct. 12	15.6	60s	3	LOT
	0.294	1.225	135.4	34.9	2012 Oct. 13	15.7	60s	2	LOT
	0.404	1.364	154.0	18.5	2012 Nov. 13	16.0	30s	5	LOT
(333358) 2001 WN1	0.131	1.109	154.1	23.0	2012 Nov. 13	16.7	30s	6	LOT
(334412) 2002 EZ2	0.211	1.193	154.9	20.8	2012 Oct. 12	18.1	60s	2	LOT
	0.214	1.193	153.5	21.9	2012 Oct. 13	18.2	60s	2	LOT
(339492) 2005 GQ21	0.198	1.165	144.5	29.8	2012 Oct. 12	16.6	60s	5	LOT
	0.198	1.167	145.6	28.9	2012 Oct. 13	16.6	60s	5	LOT
(339714) 2005 ST1	0.137	1.123	153.8	23.1	2012 Oct. 9	17.3	30s	5	LOT
(340666) 2006 RO36	0.456	1.108	91.1	64.6	2013 Oct. 2	18.5	210s, 180s	1	LOT
(341816) 2007 YK	0.554	1.456	140.4	25.5	2013 Jan. 29	18.3	300s	2	LOT
(343098) 2009 DV42	0.199	1.180	170.3	8.1	2013 Jan. 18	16.3	180s	3	SLT
	0.231	1.195	152.9	22.1	2013 Jan. 29	17.0	120s	2	LOT
(345722) 2007 BG29	0.341	1.108	102.2	60.3	2013 Jan. 29	18.4	300s	1	LOT
(349068) 2006 YT13	0.214	1.195	170.2	8.0	2013 Jan. 18	16.0	180s	3	SLT
(355256) 2007 KN4	0.889	1.843	155.0	13.3	2013 Oct. 6	18.5	210s, 180s	1	LOT
	0.930	1.874	152.6	14.2	2013 Oct. 10	18.8	300s, 240s	1	LOT
(356394) 2010 QD2	0.521	1.453	147.9	21.1	2013 Jan. 30	18.1	180s	1	LOT
(361071) 2006 AO4	0.535	1.381	122.7	38.3	2013 Jul. 10	16.4	300s	3	SLT
(363790) 2005 JE46	0.215	1.020	84.7	83.2	2013 Jul. 7	17.7	300s	2	SLT
(378610) 2008 FT6	0.487	1.278	116.7	43.4	2014 Jan. 9	18.1	270s, 240s	1	LOT
(389694) 2011 QD48	0.505	1.362	126.6	36.1	2013 Oct. 9	18.8	300s	1	LOT
(411280) 2010 SL13	0.215	1.178	151.8	23.2	2014 Jan. 9	17.5	180s, 150s	1	LOT
(441825) 2009 SK1	0.508	1.498	164.9	10.0	2013 Oct. 2	18.4	210s, 180s	1	LOT
	0.544	1.522	160.6	12.6	2013 Oct. 10	18.7	300s, 240s	1	LOT
2002 TY68	0.273	1.230	144.3	28.3	2012 Oct. 12	17.7	60s	4	LOT
2005 RQ6	0.262	1.151	119.0	49.5	2013 Oct. 3	18.1	210s, 180s	1	LOT
	0.241	1.125	116.8	52.2	2013 Oct. 20	17.8	210s, 180s	1	LOT
2010 TN54	0.204	1.198	155.3	20.6	2013 Sep. 1	17.2	300s	2	SLT
2010 XZ67	0.086	1.063	156.6	21.6	2014 Jan. 9	15.6	180s, 150s	1	LOT
2011 WV134	0.196	1.153	132.1	40.7	2012 May 23	15.4	30s	8	LOT
2012 ER14	0.101	1.076	138.2	38.2	2013 Oct. 10	17.4	300s, 240s	1	LOT
2013 SO19	0.175	1.166	160.8	16.4	2013 Oct. 6	19.2	300s, 240s	1	LOT
2013 UH9	0.190	1.040	100.4	69.3	2013 Nov. 17	17.8	150s, 120s	1	LOT

i. Geocentric distance; ii. Heliocentric distance; iii. Solar elongation; iv. Phase angles; v. one set comprises of every single exposure of B, V, R, I bands.
The values of i to iv are based exactly at 16:00 UT on each observation date.

B. The figure panels of relative reflectance spectra of 87 NEAs

The panels display the individual relative-reflectance spectra of 87 NEAs as well as their classified taxonomic types in comparison to the corresponding template spectra with dashed lines. The panels are listed by the order of asteroid numbers and the 7 taxonomic templates are also labeled with the different colors respectively.

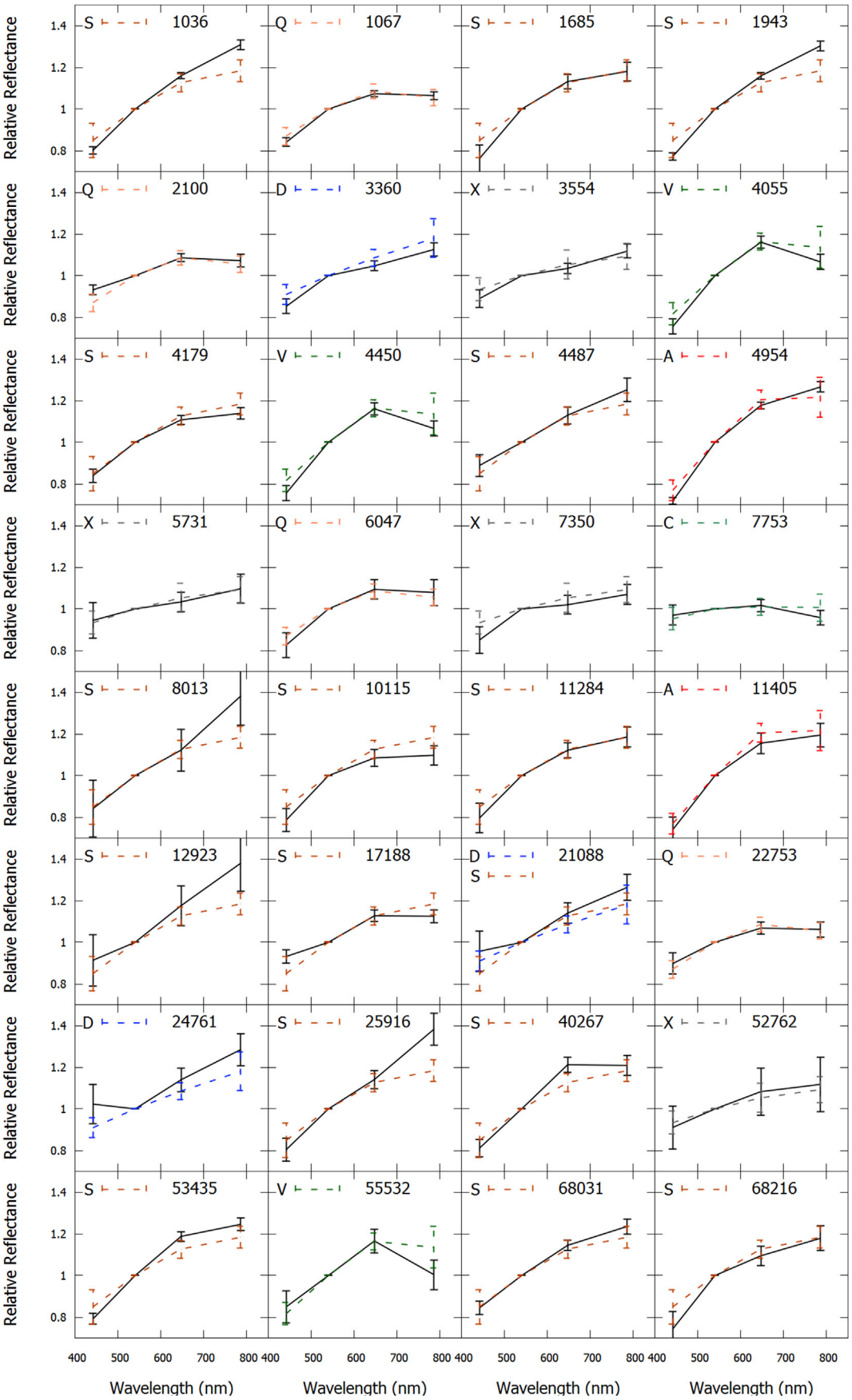
S 1036
Q 1067
S 1685
S 1943
Q 2100
D 3360
X 3554
V 4055
S 4179
V 4450
S 4487
A 4954
X 5731
Q 6047
X 7350
C 7753
S 8013
S 10115
S 11284
A 11405
S 12923
S 17188
D 21088
S
Q 22753
D 24761
S 25916
S 40267
X 52762
S 53435
V 55532
S 68031
S 68216
Relative Reflectance
Wavelength (nm)
0.8
1
1.2
1.4
400
500
600
700
800

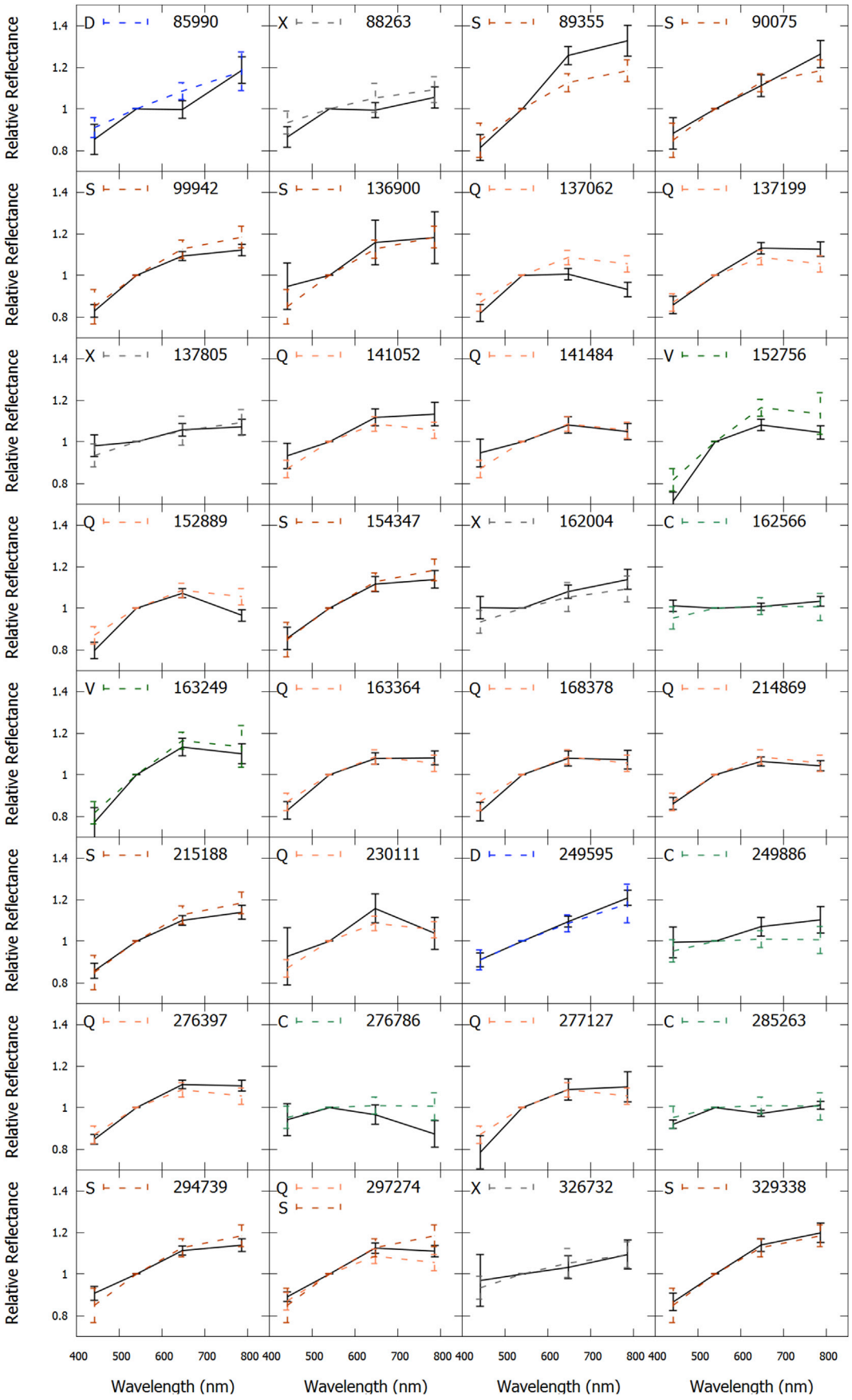
D 85990
X 88263
S 89355
S 90075
S 99942
S 136900
Q 137062
Q 137199
X 137805
Q 141052
Q 141484
V 152756
Q 152889
S 154347
X 162004
C 162566
V 163249
Q 163364
Q 168378
Q 214869
S 215188
Q 230111
D 249595
C 249886
Q 276397
C 276786
Q 277127
C 285263
S 294739
Q 297274
S
X 326732
S 329338
Relative Reflectance
Wavelength (nm)
400
500
600
700
800
0.8
1
1.2
1.4

(*continued*).

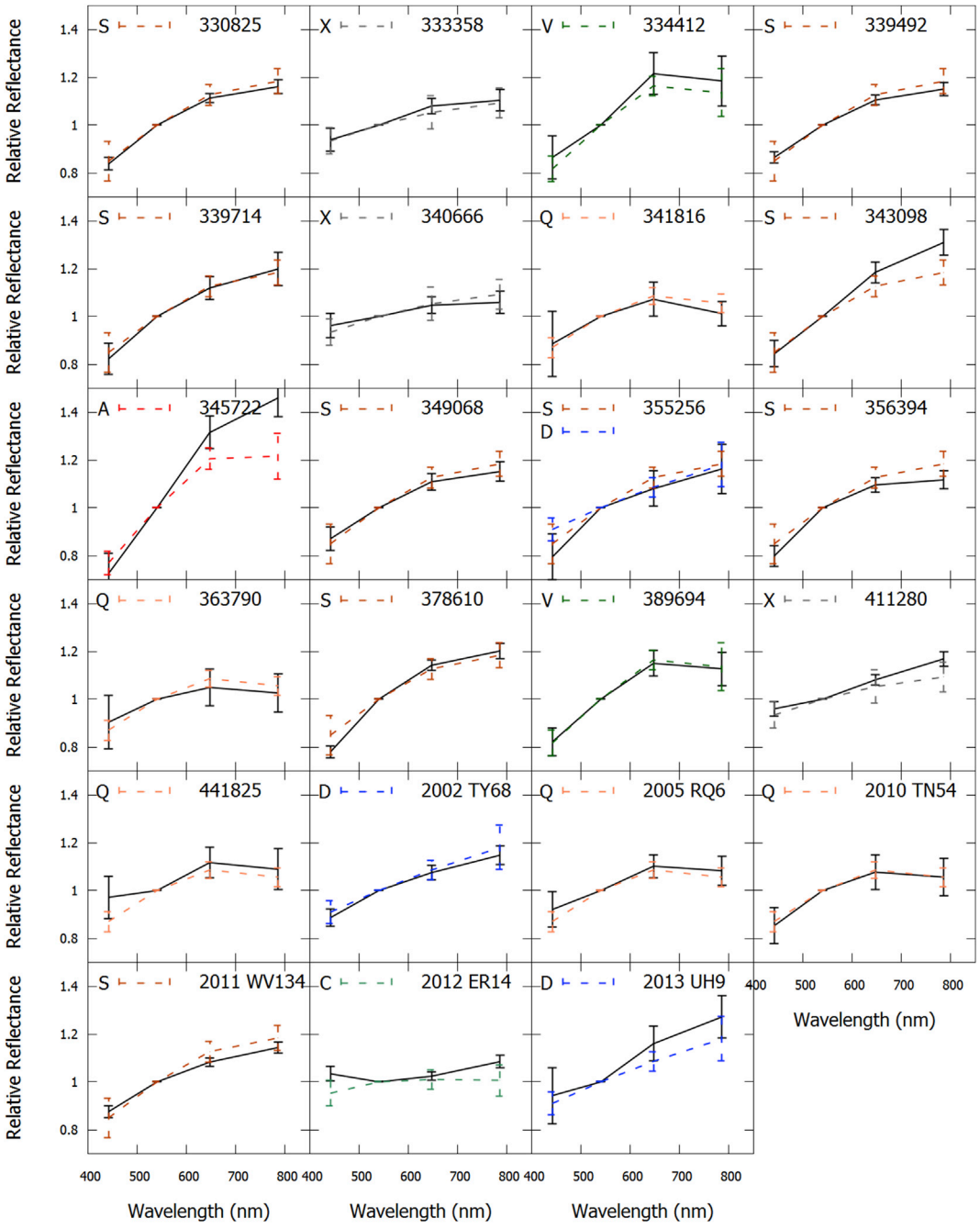

(*continued*).

C. The elaborations of observation results for individual NEAs in this paper

Here are the elaborations of our results and some comparisons with the previous reports.

The C-D-X cluster

The C-D-X cluster shown in Fig. 3.a consists of non-silicate NEAs without evident spectral features of absorption bands. Our classifications in this cluster are described below as C-, D-, and X-complexes respectively.

The C-complex

There are six members in this group.

(7753) 1988 XB: It was classified as B-type in previous spectroscopic survey (Xu et al., 1995; Bus and Binzel, 2002; Binzel et al., 2004). Since the C-complex we defined here includes the B-type subgroup as well, our classification is consistent with the previous result.

(162566) 2000 RJ34: With B-V = 0.755 ± 0.136, V-R = 0.400 ± 0.032, and R-I = 0.436 ± 0.057, Ye (2011) classified this object to be X-type. We classified it to be C-type instead on the basis of the slope of the SED. It has a low albedo (0.07) according to the NEOWISE observations (Mainzer et al., 2011).

(249886) 2001 RY11: This is a new measurement. By assuming the average albedo (0.13 ± 0.05) of the C-complex (Thomas et al., 2011), the diameter can be estimated to be 1.01–1.56 km.
(276786) 2004 KD1: This is a new measurement. With the average albedo of the C-complex, its size is estimated to be 0.88–1.36 km.
(285263) 1998 QE2: It was recognized as a binary asteroid by radar imaging observation with an albedo of 0.06 (Springmann et al., 2014). Its color indices from Hicks et al. (2013a) are B-V = 0.706 ± 0.013, V-R = 0.353 ± 0.008, and R-I = 0.374 ± 0.006. These values are close to our results. Hicks et al. (2013b) identified this object to be of Ch-type.
2012 ER14: This is a new measurement. The slopes of this NEA are between those of the C- and X-complex. It is classified to be C-complex according to the decision tree (Fig. 4). Its size is 0.24–0.37 km from using an average albedo of 0.13 ± 0.5.

The X-complex

There are 12 NEAs in this group from our observations. It is noted that the X-type objects include those classified to be E-, M- and P-type by Tholen (1984). They have rather different albedo values, namely, E-type has the highest value ≥ 0.3, M-type ~0.1–0.2 and P-type ≤ 0.1.

(3554) Amun: It was classified to be M-type (Gradie and Tedesco, 1987), X-type (Somers et al. (2010), and P-type (Thomas et al., 2014), respectively, in previous studies. It is basically in the CDX-cluster domain from our Lulin measurement. Mainzer et al., 2014) reported an albedo value of 0.142 ± 0.065 from the NEOWISE observations. The D-type designation requiring very low albedo (~0.07) can be excluded. This object could therefore be classified as M-type.
(5731) Zeus: This is a new measurement. The albedo from the NEOWISE measurements is 0.031 (Mainzer et al., 2011). This object may belong to P-type, which has the lowest albedo by the Tholen classification scheme within the X-complex.
(7350) 1993 VA: Our taxonomic classification is consistent with the C- or X-type designation from the spectroscopic observations by Thomas et al. (2014). The albedo derived by NEOWISE is 0.05 (Mainzer et al., 2011). This means that 1993 VA is likely a P-type object.
(52762) 1998 MT24: Our photometric results are in agreement with the previous classification of X-type (Whiteley, 2001; Hicks et al., 2013c). The earlier photometry, B-V = 0.713 ± 0.038, V-R = 0.41 ± 0.03, and R-I = 0.401 ± 0.016 (Hicks et al., 2013c) are also very close to ours. 1998 MT24 has a low albedo reported to be 0.052 (Pravec et al., 2012) from WISE thermal observations. It can be classified as P-type.
(88263) 2001 KQ1: This is a new measurement. The color indices from the Lulin observations have large error bars. On the basis of its spectral slopes and the decision tree, we classified it to be closer to the X-type than the C-type. This object has a low albedo of 0.048 from NEOWISE (Mainzer et al., 2011) and hence is likely to be a P-type.
(137805) 1999 YK5: It was previously classified to be X-type by SMASS II (Bus and Binzel, 2002) and RQ-type by photometry with color indices of B-V = 0.908 ± 0.035, V-R = 0.390 ± 0.051, and R-I = 0.314 ± 0.062 (Ye, 2011). However, out results are very different from the latter work. The albedo of 0.027 from NEOWISE (Mainzer et al., 2011) is extremely low compared to the R/Q-type asteroids in the S-cluster. Therefore, 1999 YK5 could be likely of P-type in the X-complex.
(162004) 1991 VE: This is a new measurement. The situation is similar to (88263) 2001 KQ1 in that the spectral slope is between the X- and D-type. We assigned it to be the X-type on the basis of our selection criterion. Without an albedo measurement, it could vary between 0.02 and 0.75 as suggested for the X-complex (Thomas et al., 2011). This means that its size is between 0.46 and 2.83 km.
(326732) 2003 HB6: This is a new measurement. It has no albedo measurements. As a consequence, its size could be between 0.46 and 2.83 km because of the large variation in the albedo values of the X-type objects.
(333358) 2001 WN1: It was reported to be C-type with photometric colors, B-V = 0.703 ± 0.044, V-R = 0.402 ± 0.023, and R-I = 0.336 ± 0.012 (Hicks and Dombroski, 2012). Although we classified 2001 WN1 to be X-complex, the spectral slope obtained by Hicks and Dombroski (2012) indicated that it could be Xc-type also. There is no albedo measurement, and its size is estimated to be 0.19–1.18 km as described above.
(340666) 2006 RO36: This is a new measurement. Its size is estimated to be 0.42–2.59 km as constrained by the albedo range of the X-type objects.
(411280) 2010 SL13: This is a new measurement. Its size is estimated to be 0.21–1.30 km as constrained by the albedo range of the X-type objects.
2013 SO10: Due to the lack of the V-R index, we can only use the other two color indices for its taxonomic classification. Its B-V index falls into the region of the C/D/X-cluster and it has a slightly higher slope at the red end. It is more likely to belong to the X-complex and the D-complex according to the priority setting scheme. In the absence of published albedo value, its size is estimated to be 0.07–0.41 km for an X-type object.

The D-complex

There are seven NEAs in this group.

(3360) Syrinx: This is a new measurement. The published albedo of 0.07 (Veeder et al., 1989) is consistent with our D-type classification.
(21088) Chelyabinsk: Previously spectroscopic observations indicted that it is SI-type (de Leo'n et al., 2010), A-type (Thomas et al., 2014). Photometric measurements by Ye (2011) assigned it to be S-type. The Lulin data showed that it could be a D-type NEA. It is noted that the B-V index is different that of the measurements of Ye (2011), perhaps because of our larger error bar in the B-band. The definite taxonomic classification would require future observations.
(24761) Ahau: It was previously classified to be S-type by photometric observations with B-V = 0.835 ± 0.023, V-R = 0.469 ± 0.008, and R-I = 0.403 ± 0.008 (Ye, 2011), and also C/X-complex by NIR spectroscopic observations (Thomas et al., 2014). Our Lulin results agree with the second one since they belong to the same group of C/D/X-cluster. There is no albedo measurement. An average albedo value of 0.02 ± 0.01 for the D-type objects (Thomas et al., 2011) would lead to a size of 2.30–4.61 km.
(85990) 1999 JV6: Bus and Binzel (2002) classified this object to be Xk-type according to the SMASS II database. Our designation of D-type is consistent with this previous result since they belong to the same C/D/X-cluster. The low albedo of 0.095 (Mainzer et al., 2011) is in agreement with the D-type classification also.
(249595) 1997 GH28: This is a new measurement. In lieu of published albedo values, its size is estimated to be 1.92–3.83 km.
2002 TY68: This is a new measurement. There is no albedo measurement either. By assuming the D-type mean albedo from Thomas et al. (2011), we estimated the diameter of this object to be 1.21–2.42 km.
2013 UH9: This is a new measurement. There is no published albedo value either. We estimated its size to be 1.27–2.53 km following the same procedure as before.

The S-Cluster

The S-cluster shown in Fig. 3.a consists of the silicate NEAs with obvious absorption features, especially in the section of SED (I-band) approaching to 1 μm. The S-complex and Q-complex objects, which are of similar compositions but differ in the level of space weathering effect together account for a majority of the NEA population. Hence we combined them as a larger group, namely, S/Q-group hereafter. We will have more analysis about S/Q-group in section 5. Our classifications are described below as S-, Q-, A-, V-complexes respectively.

The S-complex

There are 34 NEAs in this group.

(1036) Ganymed: This large NEA of 30-km size was previously classified to be S-type by both photometric measurements (Velichko and Magnusson, 2012) and spectroscopic observations (Whiteley, 2001; Bus and Binzel, 2002; Binzel et al., 2004; Hicks et al., 2011; Fieber-Beyer et al., 2011). The color indices and taxonomic type are in excellent agreement with the Lulin results.
(1685) Toro: It was classified to be an S-type NEA by SMASS observations (Binzel et al., 2004) and photometric measurements by Rabinowitz (1998); Sq-type by DeMeo et al. (2014). The Lulin results are compatible with these earlier works.
(1943) Anteros: It was before classified to be L-type (Binzel et al., 2004), S-type (Thomas et al., 2011) and Sw-type (Thomas et al., 2014). Since our definition of the S-complex contains the Sw- and L-type (see Table 3), The Lulin results are compatible with these earlier works.
(4179) Toutatis: This NEA has many observational results, both by photometry and spectroscopy. It was classified to be S-type (Howell et al., 1994; Xu et al., 1995; Lupishko et al., 1995; Davies et al., 2007; Reddy et al., 2012b) and Sk-type (Binzel et al., 2004). These taxonomic classifications and the color indices reported by Rabinowitz (1998) are in accordance with our result.
(4487) Pocahontas: This is a new measurement. There is no albedo measurement. Taking the mean value of S-type albedo as 0.26 ± 0.03 (Thomas et al., 2011), its size can be estimated to be about 0.80–0.92 km.
(8013) Gordonmoore: It was classified to be Sr-type by Lazzarin et al. (2010) which is in agreement with the Lulin results even though our data have large error bars. It has high spectral slope in the range of R-I bands. Nevertheless, the other two spectral slopes from B to R band are closer to those of the S-complex.
(10115) 1992 SK: It was classified to be a member of the S-complex (Binzel et al., 2004; DeMeo et al., 2014) and Sq-type (Thomas et al., 2014). Our Lulin results are compatible with these previous results.
(11284) Belenus: Hicks et al. (2013d) classified this object to be S-type with color indices: $B0V = 0.897 \pm 0.165$; $V\text{-}R = 0.47 \pm 0.052$ and $R\text{-}I = 0.33 \pm 0.014$. The R-I index of Hicks et al. (2013d) has a small difference from the Lulin value, but the taxonomic type is in general agreement with each other. With a nominal S-type albedo, it size can be estimated to be 0.58–0.67 km.
(12923) Zephyr: It was previously classified to be S-type (Binzel et al., 2004; Thomas et al., 2014). Although our measurements of its color indices have large error bars, we can still classify it as S-complex following our decision tree.
(17188) 1999 WC2: This is a new measurement.
(25916) 2001 CP44: It was classified to be Sq/Q-type by NIR spectroscopy before (Thomas et al., 2014). Our results showed slightly different classification, but they basically belong to the same S/Q-group.
(40267) 1999 GJ4: It was previously reported to be Sq-type (Binzel et al., 2004) which is not too different from our S-complex classification and still in the same S/Q-group.
(53435) 1999 VM40: It was classified to be S-type (Binzel et al., 2004) and Srw-type (Thomas et al., 2014), which are all parts of the S-complex in agreement with our classification.
(68031) 2000 YK29: This is a new measurement. With a nominal S-type albedo, its size can be estimated to be 0.58–0.67 km.
(68216) 2001 CV26: It has the near-infrared spectroscopic observation (Reddy, 2010). It was previously classified to be R-type by Ye (2011), Sq-type by Thomas et al. (2014) and S-complex by DeMeo et al. (2014). The previous two are different from our S-complex designation here, yet they are all parts of the S-cluster.
(89355) 2001 VS78: It was previously classified to be S-type (Binzel et al., 2004) and Sr-type (Thomas et al., 2014). They are both compatible with our S-complex designation.
(90075) 2002 VU94: This is a new measurement. The spectral slopes from the Lulin observations are intermediate between the D- and S-type. The S-complex classification is supported by the albedo value of 0.197 determined by NEOWISE (Nugent et al., 2015).
(99942) Apophis: This famous PHA was detected to be Sq-type by Binzel et al. (2009). It is generally in agreement with our results. The detected albedo is about 0.3 (Mu"ller et al., 2014).
(136900) 1998 HL49: This is a new measurement. With a nominal S-type albedo, it size can be estimated to be 0.84–0.96 km.
(154347) 2002 XK4: This object was previously observed by NIR spectroscopy and classified to be S-complex (Lazzarin et al., 2010). With a nominal S-type albedo, it size can be estimated to be 1.5–1.8 km.
(215188) 2000 NM: It was previously classified to be Sr-type by spectroscopy (Binzel et al., 2004) and R-type by photometry (Dandy et al., 2003).
(219071) 1997 US9: We only have two color indices of B-V and V-I for this NEA. Its hyper-reddish end of the I band probably indicates a spectral signature of the A-type asteroids, but the B-V slope is more like that of the S-complex. Our S-complex classification is in line with the S-type designation by Whiteley (2001) and Q-type (Binzel et al., 2004; Thomas et al., 2014: DeMeo et al., 2014).
(262623) 2006 WY2: This is a new measurement. We only measured two color indices, namely, B-V and V-I, of this NEA. Without the V-R slope we could still approximately classify it to be of S-complex because of the trends of the other two slopes.
(294739) 2008 CM: This is a new measurement. With a nominal S-type albedo, it size can be estimated to be 0.84–0.96 km.
(329338) 2001 JW2: This is a new measurement. With a nominal S-type albedo, it size can be estimated to be 0.36–0.42 km.
(330825) 2008 XE3: This potentially binary NEA was classified to be S-type by photometric observations (Hicks et al., 2012a). The reported color indices are similar to our Lulin results and the classifications are identical. With a nominal S-type albedo, it size can be estimated to be 1.33–1.52 km.
(339492) 2005 GQ21: This is a new measurement. With a nominal S-type albedo, it size can be estimated to be 0.56–0.64 km.
(339714) 2005 ST1: This is a new measurement. With a nominal S-type albedo, it size can be estimated to be 0.20–0.23 km.
(343098) 2009 DV42: The R-I slope is similar to the reddish feature of the A-type objects. However, the overall SED trends fit better with those of the S-complex according to the decision tree (see Fig. 4). Both of the taxonomic type and albedo have not been investigated before. With a nominal S-type albedo, it size can be estimated to be 0.44–0.50 km.

(349068) 2006 YT13: It was classified to be A/R-type by photometry, with B-V = 1.042 ± 0.088 and V-R = 0.475 ± 0.057 (Ye, 2011). These color indices are somewhat different from the Lulin results even though they are consistent with our S-cluster classification. With a nominal S-type albedo, it size can be estimated to be 0.53–0.61 km.
(355256) 2007 KN4: This is a new measurement. The corresponding SED has rather large error bars and the B-V slope is higher than that of the D-complex but similar to the S-complex value. We designated two possible taxonomic types with the S-type to be followed by the D-type. It is interesting to note that 2007 KN4 is the only object in our sample with the Jovian Tisserand parameter ($T_J = 2.77$) being less than 3.0. This means that this NEA could be an extinct comet (Carusi et al., 1987). We would need more observations in future to determine whether this object should be classified as D-type instead as appropriate to a cometary nucleus. For the present moment, with a nominal S-type albedo, it size can be estimated to be 1.06–1.21 km.
(356394) 2010 QD2: This is a new measurement. With a nominal S-type albedo, it size can be estimated to be 0.80–092 km.
(378610) 2008 FT6: This is a new measurement. With a nominal S-type albedo, it size can be estimated to be 0.80–0.92 km.
2011 WV134: Previous photometric observations indicated that it is an S-type (Hicks et al., 2012b) in agreement with our Lulin result. With a nominal S-type albedo, it size can be estimated to be 0.88–1.01 km.

The Q-complex

There are 24 NEAs in this group.

(1627) Ivar: It was previously classified to be S-type by spectroscopic observations (Bus and Binzel, 2002; Binzel et al., 2004; Davies et al., 2007) and photometry, with B-V = 0.80 ± 0.02, V-R = 0.45 ± 0.01, and R-I = 0.34 ± 0.01 (Hahn et al., 1989; Velichko and Rikhteghar, 2011). These color indices are similar to the Lulin results. However, our classification is slightly different.
(2100) Ra-Shalom: It was classified to be K-type (Shepard et al., 2008), Sr-type (Harris et al., 1998), and C-type (Binzel et al., 2004), which are very different from our present classification. Its SED in the Figure of Appendix B shows that the spectral slope of B-V is flatter and similar to that of the C-/X-complex. On the other hand, the slopes from V to I band are close to those of the Q-complex with absorption feature near 1 μm.
(4450) Pan: It was classified to be S-type by photometric observations with
B-V = 0.82 ± 0.02, V-R = 0.48 ± 0.02 and R-I = 0.28 ± 0.02 (Carbognani, 2008) and S/Sr-type by spectroscopy (Perna et al., 2016). Our classification is different but in the general S/Q-group. There is no albedo measurement. With a nominal Q-type albedo of 0.29 ± 0.03 (Thomas et al., 2011), it size can be estimated to be 0.9–1.1 km.
(6047) 1991 TB1: This NEA was classified to be S-type before (Binzel et al., 2004; DeMeo et al., 2009; Thomas et al., 2014). In the Lulin measurements, the R-I spectral slope is better fit by the Q-complex value.
(22753) 1998 WT: It was classified to be Q-type (Whiteley, 2001) and Sq-type (Thomas et al., 2014). They are both consistent with our result.
(137062) 1998 WM: It was classified to be Sq-type (Binzel et al., 2004; Thomas et al., 2014) and Q-type (DeMeo et al., 2014). They are both consistent with our result.
(137199) 1999 KX4: It was classified to be Sq-type by spectroscopy (Hicks et al., 2013b). With a nominal Q-type albedo, it size can be estimated to be 1.0–1.2 km.
(141052) 2001 XR1: Our result is consistent with the taxonomic identification of Sq-type by Binzel et al. (2004) and Thomas et al. (2011).
(141484) 2002 DB4: It was classified to be S-type (Michelsen et al., 2006) and S-complex (Lazzarin et al., 2010). There is no albedo measurement. With a nominal Q-type albedo, it size can be estimated to be 1.2–1.5 km.
(152889) 2000 CF59: This is a new measurement.
(163364) 2002 OD20: It was reported to be Sq-type by Hicks et al. (2013b). With a nominal Q-type albedo, it size can be estimated to be 0.4–0.5 km.
(168378) 1997 ET30: This is a new measurement. With a nominal Q-type albedo, it size can be estimated to be 1.04–1.24 km.
(214869) 2007 PA8: It was classified to be Q-type (Kuroda et al., 2014; Fornasier et al., 2015; Sanchez et al., 2015; Perna et al., 2016), S-type (Godunova et al., 2013), and Xc-type by broad-band photometry (Hicks et al., 2012c). The albedo was detected to be 0.29±0.14 (Brozović et al., 2017).
(230111) 2001 BE10: It was classified to be S-complex by spectroscopic observation (DeMeo et al., 2014) and R-type by photometry (Ye, 2011) with color indices: B-V = 0.956 ± 0.087, V-R = 0.458 ± 0.035 and R-I = 0.412 ± 0.101. These identifications together with our Lulin result are basically in the S-cluster.
(276397) 2002 XA40: This is a new measurement. With a nominal Q-type albedo, it size can be estimated to be 0.91–1.08 km.
(277127) 2005 GW119: It was classified to be Sq-type (Ieva et al., 2014) in accordance with our result. With a nominal Q-type albedo, it size can be estimated to be 0.43–0.52 km.
(297274) 1996 SK: It was identified to be S-type with apparent rotational color variability by Lin et al. (2014). Our present Lulin measurement showed that its spectral slope is intermediate between S-type and Q-type thus indicating that this NEA probably has inhomogeneous surface composition as reported before. We classified 1996 SK with the first taxonomic type to be Q-complex and second to be S-complex according to the decision tree (see Fig. 4). With a nominal Q-type albedo, it size can be estimated to be 1.09–1.3 km.
(341816) 2007 YK: This is a new measurement. With a nominal Q-type albedo, it size can be estimated to be 0.76–0.9 km.
(361071) 2006 AO4: This is a new measurement. With a nominal Q-type albedo, it size can be estimated to be 1.98–2.36 km.
(363790) 2005 JE46: It was classified to be C/X/D-complex by spectroscopic observations (Thomas et al., 2014). The spectral slopes between B to R in Figure of Appendix B are indeed similar to those of the X-complex, but the R-I slope is more like that of the Q-complex. With a nominal Q-type albedo, it size can be estimated to be 0.69–0.82 km.
(441825) 2009 SK1: This is a new measurement. With a nominal Q-type albedo, it size can be estimated to be 0.52–0.62 km.
2005 RQ6: It was previously classified to be S/Sr-type (DeMeo et al., 2014) in the same S/Q-group as our identification. With a nominal Q-type albedo, it size can be estimated to be 0.4–0.47 km.
2010 TN54: This is a new measurement. With a nominal Q-type albedo, it size can be estimated to be 0.35–0.41 km.
2010 XZ67: This is a new measurement. The V-R color index is missing. The taxonomic characterization can be done by consideration of the partial SED which is more likely to be Q-complex than the V-complex. With a nominal Q-type albedo, it size can be estimated to be 0.27–0.32 km.

The A-complex

There are three NEAs in this group.

(4954) Eric: It was classified to be S-type by both photometry (Rabinowitz, 1998) and SMASS observations (Binzel et al., 2004). Yet our Lulin measurements indicated that its spectral slopes with reddening feature close to the A-complex slopes. However, according to Gietzen et al. (2012), the NIR spectra of 4954 Eric exhibits an absorption feature at 2 micron indicating the presence of clinopyroxene. Because A-type does not have the pyroxene absorption band, the classification here might be wrong and this NEA should be classified as S-type.
(11405) 1999 CV3: It was classified to be Sq-type by SMASS database. But the Lulin result showed that it is close to A-complex.
(354722) 2007 EG29: This is a new measurement.

The V-complex

Some of the V-type NEAs are supposed to be small members of the Vesta family got transported into the orbital region of the terrestrial planets. Their spectral slopes between B to R are similar to those of the S-complex. But there is a significant descending slope between the R and I band because of a deeper absorption feature close to 1 μm. There are six objects in this group from our Lulin observations.

(4055) Magellan: It was classified to be V-type by several spectroscopic observations (Cruikshank et al., 1991; Binzel et al., 2004; Whiteley, 2001; Sanchez et al., 2013; Thomas et al., 2014). We have exactly the same classification. The albedo was detected to be about 0.33 (Delbo et al., 2003)
(55532) 2001 WG2: It was classified to be Sk-type by SMASS observations (Binzel et al., 2004). This is different from our identification though in the same S-cluster.
(152756) 1999 JV3: It was classified to be S-type (Binzel et al., 2004) and Sa-type (Hicks et al., 2013b). They are both different from our identification though in the same S-cluster.
(163249) 2002 GT: It was classified to be Sq-type by spectroscopic observation (Hicks et al., 2013b). Its spectral slopes between V to I are intermediate between the S- and Q-type, but that of B-V is more similar to the V-type. With the nominal albedo of 0.42 ± 0.11 (Thomas et al., 2011) for the V-type NEAs, it size can be estimated to be 0.37–0.5 km.
(334412) 2002 EZ2: Our Lulin measurements have relatively large error bars, but the SED is close to that of the V-complex. In addition, the detected albedo of 0.4 by the warm Spitzer survey (Thrilling et al., 2010) is close to the mean albedo of the V-type NEAs (Thomas et al., 2011).
(389694) 2011 QD48: This is a new measurement. With the nominal albedo of the V-type asteroids, it size can be estimated to be 0.41–0.55 km.

References

Bertini, I., 2011. Main Belt Comets: a new class of small bodies in the solar system. Planet. Space Sci. 59, 365–377.
Binzel, R.P., et al., 2002. Physical Properties of Near-earth Objects. In: Asteroids III. Univ. of Arizona press, p. 255.
Binzel, R.P., et al., 2004. Observed spectral properties of near-Earth objects: results for population distribution, source regions, and space weathering processes. Icarus 170, 259–294.
Binzel, R.P., et al., 2009. Spectral properties and composition of potentially hazardous Asteroid (99942). Apophis. Icarus 200, 480–485.
Binzel, R.P., et al., 2010. Earth encounters as the origin of fresh surfaces on near- Earth asteroids. Nature 463, 331–334.
Bottke, W.F., et al., 2002. Debiased orbital and absolute magnitude distribution of the near-Earth objects. Icarus 156, 399–433.
Brozović, M., et al., 2017. Goldstone radar evidence for short-axis mod;e non-principal-axis rotation of near-Earth asteroid (214869) 2007 PA8. Icarus 286, 314–329.
Brunetto, R., et al., 2006. Modeling asteroid surfaces from observations and irradiation experiments: the case of 832 Karin. Icarus 184, 327–337.
Brunetto, R., et al., 2015. Asteroid Surface Alteration by Space Weathering Processes. Asteroid IV. University of Arizona Press, pp. 597–616.
Bus, S.J., 1999. Compositional Structure in the Asteroid Belt: results of a Spectroscopic Survey. PhD. Thesis.
Bus, S.J., Binzel, R.P., 2002. Phase II of the small main-belt asteroid spectroscopic survey. A feature-based taxonomy. Icarus 158, 146–177.
Carbognani, A., 2008. MPB. Light Curve Photometry of NEAs 4450 PAN, (170891) 2004 TY16, 2002 RC118, and 2007 VD12; 2006NM, 35, pp. 109–110.
Carry, B., et al., 2016. Spectral properties of near-Earth and Mars-crossing asteroids using Sloan photometry. Icarus 268, 340–354.
Carusi, A., et al., 1987. High-order librations of Halley-type comets. Astron. Astrophys. 187, 899–905.
Clark, B.E., et al., 2002. NEAR infrared spectrometer photometry of asteroid 433 Eros. Icarus 155, 189–204.
Cruikshank, D.P., et al., 1991. Three basaltic earth-approaching asteroids and the source of the basaltic meteorites. Icarus 89, 1–13.
Dandy, C.L., Fitzsimmons, A., Collander-Brown, S.J., 2003. Optical colors of 56 near-Earth objects: trends with size and orbit. Icarus 163, 363–373.
Davies, J.K., et al., 2007. Near-infrared spectra of 12 near-Earth objects. Icarus 186, 111–125.
de Leo'n, L., et al., 2010. Observations, compositional, and physical characterization of near-Earth and Mars-crosser asteroids from a spectroscopic survey. Astron. Astrophys 517, A23.
Delbo, M., et al., 2003. Keck observations of near-Earth asteroids in the thermal infrared. Icarus 166, 116–130, 4055 albedo.
DeMeo, F.E., Carry, B., 2013. The taxonomic distribution of asteroids from multifilter all-sky photometric surveys. Icarus 226, 723–741.
DeMeo, F.E., Carry, B., 2014. Solar System evolution from compositional mapping of the asteroid belt. Nature 505, 629–634.
DeMeo, F.E., et al., 2009. An extension of the Bus asteroid taxonomy into the near infrared. Icarus 202, 160–180.
DeMeo, F.E., Binzel, R.P., Lockhart, M., 2014. Mars encounters cause fresh surfaces on some near-Earth asteroids. Icarus 227, 112–122.
Fieber-Beyer, S.K., Gaffey, M.J., Abell, P.A., 2011. Mineralogical characterization of near-Earth asteroid (1036). Ganymed. Icarus 212, 149–157.
Fornasier, S., et al., 2015. The potentially hazardous asteroid (214869) 2007 PA8: an unweathered L chondrite analogue surface. Icarus 250, 280–286.
Gietzen, K.M., 2009. Near Infrared Spectral Data for 27 Asteroids: an Investigation of Meteorite-asteroid Relationships by Using the Modified Gaussian Method. PhD thesis. University of Arkansas.
Gietzen, K.M., et al., 2012. IRTF observations of S complex and other asteroids: implicagions for surface compositions, the presence of clinopyroxenes, and their relationship to meteorites. Meteor. Planet. Sci. 47, 1789.
Godunova, V., et al., 2013. Spectrophotometric studies of near-Earth asteroids at the Terskol Observatory. EGU2013-13797-1 (Abstract).
Gradie, J.C., Tedesco, E.F., 1987. 1986 DA and 1986 EB: iron objects in near-earth orbits. Lun. Plant. Sci. Con 18, 349.
Granvik, M., et al., 2016. Super-catastrophic disruption of asteroids at small perihelion distances. Nature 530, 303–306.
Graves, K., et al., 2016. Size and Perihelion Distribution of S and Q-type Asteroid Spectral Slopes from the Near Earth Region through the Main Belt. DPS Meeting. #48, id. 510.09.
Greenstreet, et al., 2012. The orbital distribution of Near-Earth Objects inside Earth's orbit. Icarus 217, 355–366.
Hahn, G., et al., 1989. Physical studies of Apollo-Amor asteroids - UBVRI photometry of 1036 Ganymed and 1627 ivar. Icarus 78, 363–381.
Harris, A.W., et al., 1998. Thermal infrared spectrophotometry of the near-earth asteroids 2100 Ra-Shalom and 1991 EE. Icarus 135, 441–450.
Hicks, M., Dombroski, D., 2012. Physical characterization of (333358) 2001 WN1: a large, possibly water-rich, low delta-V near-Earth asteroid. The Astron. Tel. 4623.
Hicks, M., Ebelhar, S., 2013a. Broadband photometry of the large potentially hazardous asteroid 138095 (2000 DK79). The Astron. Tel. 5591.
Hicks, M., Ebelhar, S., 2013b. Broadband photometry of the potentially hazardous asteroid 2013 RH74. The Astron. Tel. 5562.
Hicks, M., Ebelhar, S., 2014a. Broad-band photometry of the potentially hazardous asteroid 2006 DP14. The Astron. Tel. 5928.
Hicks, M., Ebelhar, S., 2014b. Broadband photometry of the potentially hazardous asteroid 251346 (2007 SJ). The Astron. Tel. 5801.
Hicks, M., et al., 2011. Palomar spectroscopy of near-earth asteroids 2004 SV55, 2000 SP43, 3988 (1986 LA), 1036 Ganymed, and 2002 AG29. The Astron. Tel. 3678.
Hicks, M., et al., 2012a. Broadband photometry 330825 (2008 XE3): a potential binary near-earth asteroid. The Astron. Tel. 4591.
Hicks, M., et al., 2012b. Physical characterization of the potentially hazardous asteroid 2011 WV134. The Astron. Tel. 4251.

Hicks, M., et al., 2012c. Broadband photometry of 214869 (2007 PA8): a slowly rotating potentially hazardous asteroid. The Astron. Tel. 4625.
Hicks, M., et al., 2012d. Broadband photometry of the near-earth asteroid 136993 (1998 ST49). The Astron. Tel. 4588.
Hicks, M., et al., 2012e. Broadband photometry of the potentially hazardous asteroid 329614 (2003 KU2). The Astron. Tel. 4262.
Hicks, M., et al., 2012f. Broadband photometry of 2012 LZ1: a large, dark potentially hazardous asteroid. The Astron. Tel. 4252.
Hicks, M., et al., 2012g. Broadband photometry of 2007 LE: a binary near-earth asteroid. The Astron. Tel. 4188.
Hicks, M., et al., 2012h. Optical photometry of 2012 EG5: constraints on taxonomy and spin rate. The Astron. Tel. 4016.
Hicks, M., et al., 2013a. BVRI photometry of the potentially hazardous asteroid 285263 (1998 QE2). The Astron. Tel. 5121.
Hicks, M., et al., 2013b. Palomar spectroscopy of near-earth asteroids 137199 (1999 KX4), 152756 (1999 JV3), 163249 (2002 GT), 163 364 (2002 OD20), and 285263 (1998 QE2). The Astron. Tel. 5132.
Hicks, M., et al., 2013c. Broad-band photometry of 52762 (1998 MT24). The Astron. Tel. 5306.
Hicks, M., et al., 2013d. Broadband photometry of 11284 Belenus: a large low delta-V near-Earth asteroid. The Astron. Tel. 4969.
Hicks, M., et al., 2013e. Broadband photometry of the potentially asteroid 277475 (2005 WK4) and corrected 52762 (1998 MT24) colors. The Astron. Tel. 5311.
Hicks, M., et al., 2014a. Broad-band photometry of the near-earth asteroid 2014 CR. The Astron. Tel. 5955.
Hicks, M., et al., 2014b. Broad-band photometry of NHATS target 387733 (2003 GS). The Astron. Tel. 6090.
Howell, E.S., et al., 1994. Visible and near-infrared spectral observations of 4179 Toutatis. Icarus 111, 468–474.
Hsieh, H.H., Jewit, D., 2006. A population of comets in the Main Asteroid Belt. Science 312, 561.
Ieva, S., et al., 2014. Low Delta-V Near-Earth Asteroids: a survey of suitable targets for space missions. Astron. Astrophys. 569, A59.
Ishiguro, M., et al., 2007. Global mapping of the degree of space weathering on asteroid 25143 Itokawa by Hayabusa/AMICA observations. Meteoritics Planet Sci. 42, 1791–1800.
Ivezic, Z., et al., 2001. AJ. Solar System Objects Observed in the Sloan Digital Sky Survey Commissioning Data, 122, pp. 2749–2784.
Jacobson, S.A., Scheeres, D.J., 2011. Dynamics of rotationally fissioned asteroids: source of observed small asteroid systems. Icarus 214, 161–178.
Jones, T.D., et al., 1990. The composition and origin of the C, P, and D asteroids - water as a tracer of thermal evolution in the outer belt. Icarus 88, 172–192.
Kuroda, D., et al., 2014. Visible-wavelength spectroscopy of subkilometer-sized near-Earth asteroids with a low delta-v. PASJ 66, 51.
Landolt, A.U., 1992. UBVRI photometry standard stars in the magnitude range 11.5<V<16.0 around the celestial equator. Astron. J. 104, 340–371.
Lang, D., et al., 2010. Astrometry.net: blind astrometric calibration of arbitrary astronomical images. Astron. J. 139, 1782–1800.
Lazzarin, M., et al., 2005. Spectroscopic investigation of near-earth objects at telescopio nazionale Galileo. Mon. Not. R. Astron. Soc. 359, 1575–1582.
Lazzarin, M., Marchi, S., Magrin, S., 2010. Spectroscopic Investigation of Near-earth Objects. SINEO Database.
Lazzaro, D., et al., 2004. S3OS2: the visible spectroscopic survey of 820 asteroids. Icarus 172, 179–220.
Lim, L.F., et al., 2012. The near-earth encounter of asteroid 308635 (2005 YU55). In: Thermal IR Observations. AAS 2012 DPS Meeting. #44, id.305.01L.
Lin, C.-H., et al., 2014. Detection of large color variation of potentially hazardous asteroid (297274) 1996 SK. Res. Astron. Astrophys. 14, 311.
Lin, H.-W., et al., 2015. A search for subkilometer-sized ordinary chondrite like asteroids in the main-belt. Icarus 254, 202–212.
Lupishko, D.F., et al., 1995. UBVRI-polarimetry of asteroid 4179 Toutatis. Icarus 113, 200–205.
Mainzer, A., et al., 2011. Preliminary results from NEOWISE: an enhancement to the wide-field infrared survey explorer for solar system science. Astron. Astrophys. J. 731, 53M.
Mainzer, A., et al., 2014. Initial performance of the NEOWISE reactivation mission) (prel.diameters & albedos for 61 NEOs. Astrophys. J. 792, 30.
Michelsen, R., et al., 2006. Spectroscopy of near-Earth asteroids. Astron. Astrophys. 451, 331–337.
Morbidelli, A., Vokrouhlicky', D., 2003. The Yarkovsky-driven origin of near-Earth asteroids. Icarus 163, 120–134.
Mu''ller, T.G., et al., 2014. Thermal infrared observations of asteroid (99942) Apophis with herschel. Astron. Astrophys. 566, A22.
Nakamura, T., et al., 2011. Itokawa dust particles: a direct link between S-Type asteroids and ordinary chondrites. Science 333, 1113.
Nesvorný, D., et al., 2010. Do planetary encounters reset surfaces of near Earth asteroids? Icarus 209, 510–519.
Nichols, C.R., 1993. Volatile Products from Carbonaceous Asteroids. In Resources of Near-earth Space, Part III. No. 21. University of Arizona Press.
Nugent, C.R., et al., 2015. NEOWISE reactivation mission year one: preliminary asteroid diameters and albedos. Astrophys. J. 814, 117, 13 pp.
Perna, D., et al., 2016. Grasping the nature of potentially hazardous asteroids. Astron. J. 151, 11, 14pp.
Polishook, D., et al., 2014. Observations of fresh and weathered surfaces on asteroid pairs and their implications on the rotational-fission mechanism. Icarus 233, 9–26.
Popescu, M., et al., 2014. Spectral properties of the largest asteroids associated with Taurid Complex. A&A 572, A106.
Pravec, P., et al., 2012. Absolute magnitudes of asteroids and a revision of asteroid albedo estimates from WISE thermal observations. Icarus 221, 365–387.
Rabinowitz, D.L., 1998. Size and orbit dependent trends in the reflectance colors of earth-approaching asteroids. Icarus 134, 342–346.
Rayner, J.T., et al., 2003. SpeX: a Medium-resolution 0.8-5.5 Micron Spectrograph and Imager for the NASA Infrared Telescope Facility, vol 115. PASP, p. 362.
Reddy, V., 2010. IRTF Near-earth Asteroid Spectra V1.0, NASA Planetary Data System, EAR-A-I0046-5-REDDYSPEC-V1.0.
Reddy, V., et al., 2012a. Composition of near-Earth Asteroid 2008 EV5: potential target for robotic and human exploration. Icarus 221, 678–681.
Reddy, V., et al., 2012b. Composition of near-earth asteroid (4179) Toutatis. Icarus 221, 1177–1179.
Rivkin, A.S., 2006. An introduction to near-earth objects. Johns Hopkins APL Technical Digest 27 (No. 2).
Rubincam, D.P., 2000. Radiative spin-up and spin-down of small asteroids. Icarus 148, 2–11.
Sanchez, J.A., Michelsen, R., Reddy, V., Nathues, A., 2013. Surface composition and taxonomic classification of a group near-Earth and Mars-crossing asteroids. Icarus 225 (Iss. 1), 131–140.
Sanchez, J.A., Reddy, V., Dykhus, M., Lindsay, S., Le Corre, L., 2015. Composition of potentially hazardous asteroid (214869) 2007 PA8: an H chondrite from outer asteroid belt. Astrophys. J. 808, 93.
Scheeres, D.J., 2015. Landslides and Mass shedding on spinning spheroidal asteroids. Icarus 247, 1–17.
Shepard, M.K., et al., 2008. Multi-wavelength observations of asteroid 2100 Ra-Shalom. Icarus 193, 20–38.
Somers, J.M., et al., 2010. Optical characterization of planetary radar targets, low-deltaV, and potentially hazardous asteroids: results from 2009-2010. DPS 42, 1316.
Springmann, A., et al., 2014. Radar derived shape model of binary near-earth asteroids (285263) 1998 QE2. Lun. Plant. Sci. Con 45, 1313.
Stuart, J.S., Binzel, R.P., 2004. Bias-corrected population, size distribution, and impact hazard for the near-Earth objects. Icarus 170, 295–311.
Tholen, D.J., 1984. Asteroid Taxonomy from Cluster Analysis of Photometry (Ph.D. Thesis).
Thomas, C.A., et al., 2011. ExploreNEOs. V. Average albedo by taxonomic complex in the near-earth asteroid population. Astron. J. 142, 85, 12pp.
Thomas, C.A., et al., 2014. Physical characterization of Warm Spitzer-observed near-Earth objects. Icarus 228, 217–246.
Thrilling, D.E., et al., 2010. EXPLORENEOs. I. Description and first results from the warm spitzer near-earth object survey. Astron. J. 140, 770–784.
Tubiana, C., et al., 2015. A&A. 2P/Encke, the Taurid Complex NEOs and the Maribo and Sutter's Mill Meteorites, vol 584, p. A97.
Veeder, G.J., et al., 1989. Radiometry of near-Earth asteroids. Astron. J. 97, 1211–1219.
Velichko, F.P., Magnusson, P., 2012. Photometry and polarimetry of the largest NEA 1036 Ganymed. Astron. Tsirk. 1575.
Velichko, F.P., Rikhteghar, A., 2011. Light curves, colours and magnitude phase dependences of the asteroids 433 Eros and 1627 Ivar. Astronomy 47, 41–43.
Vernazza, P., et al., 2008. Composition differences between meteorites and near-Earth asteroids. Nature 454, 858–860.
Volquardsen, E.L., 2007. Composition of hydrated near-Earth object (100085) 1992 UY4. Icarus 187, 464–468.
Walsh, K.J., Richardson, D.C., Michel, P., 2012. Spin-up of rubble-pile asteroids: disruption, satellite formation, and equilibrium shapes. Icarus 220, 514–529.
Whiteley, R.J., 2001. A Compositional and Dynamical Survey of the Near-earth Asteroids. PhD. Thesis. University of Hawaii.
Xu, S., et al., 1995. Small main-belt asteroid spectroscopic survey: initial results. Icarus 115 (no. 1), 1–35.
Ye, Q.-Z., 2011. BVRI photometry of 53 unusual asteroids. Astron. J. 141, 32, 8pp.